

Supplement A: Detailed micro-Raman spectroscopy and U–Pb geochronological results

A1. Spectra obtained by micro-Raman spectroscopy in the studied samples (see also Appendix C).

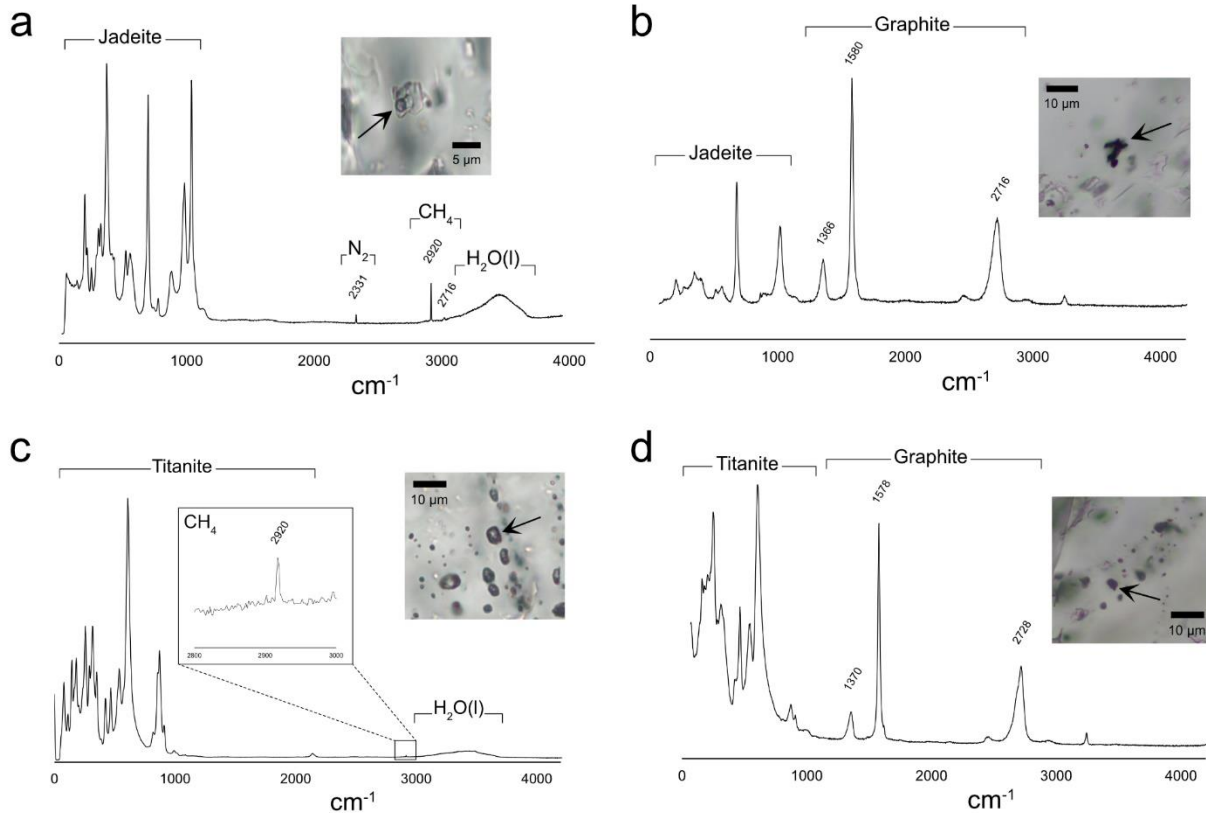


Figure S1 Raman spectra of fluid (a and c) and graphite (b and d) inclusions in (a–b) jadeite, (c–d) titanite in jadeitite sample GT1. The photomicrographs are in plane-polarized light, and they were acquired using the ZEISS ZEN core software (version 3.6).

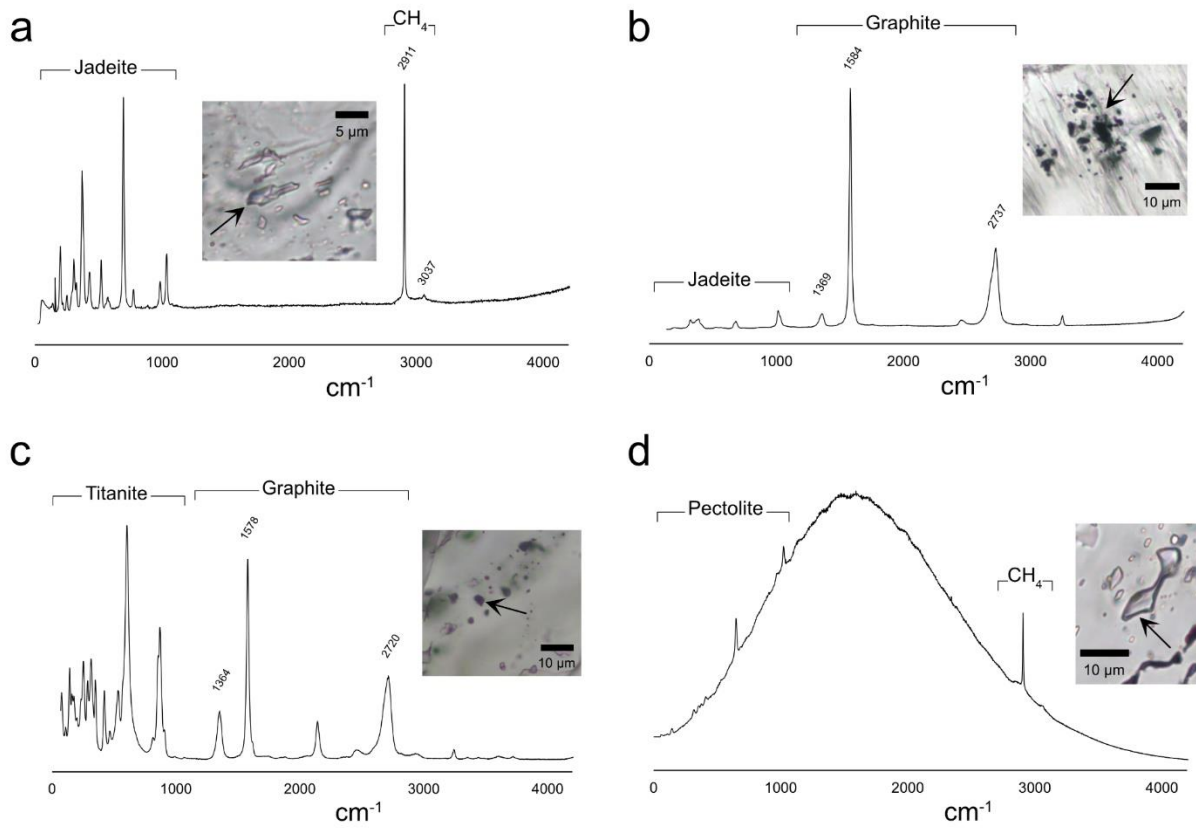


Figure S2 Raman spectra of fluid and graphite inclusions in (a–b) jadeite, (c) titanite, and (d) pectolite in jadeitite sample OSJ1002. The photomicrographs are in plane-polarized light, and they were acquired using the ZEISS ZEN core software (version 3.6).

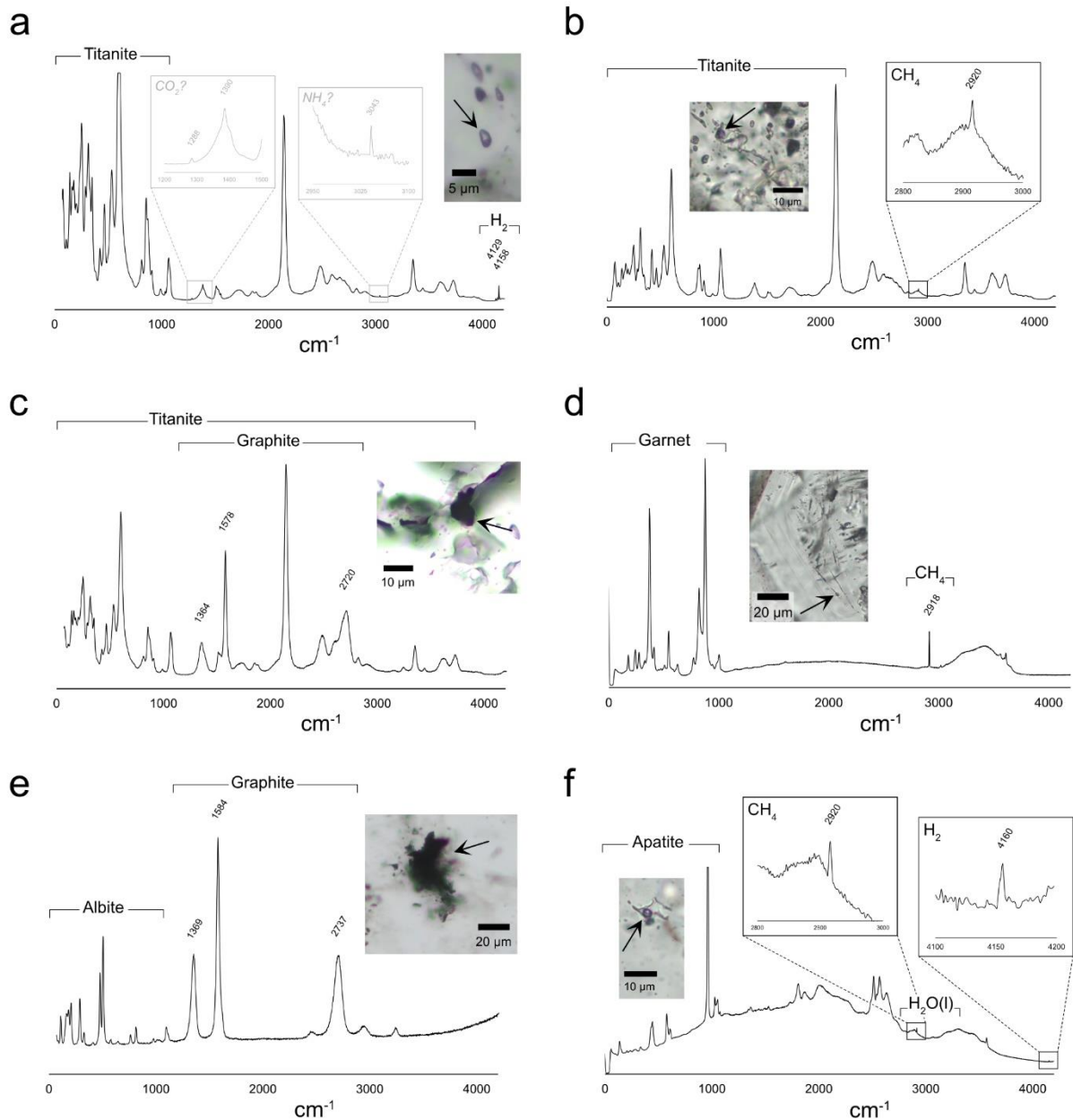


Figure S3 Raman spectra of fluid and graphite inclusions in (a–c) titanite, (d) grossular-rich garnet, (e) albite and (f) apatite in albite sample R5. The photomicrographs are in plane-polarized light, and they were acquired using the ZEISS ZEN core software (version 3.6). Gray boxes and text in panel a indicate uncertainty in the identification of specific chemical species.

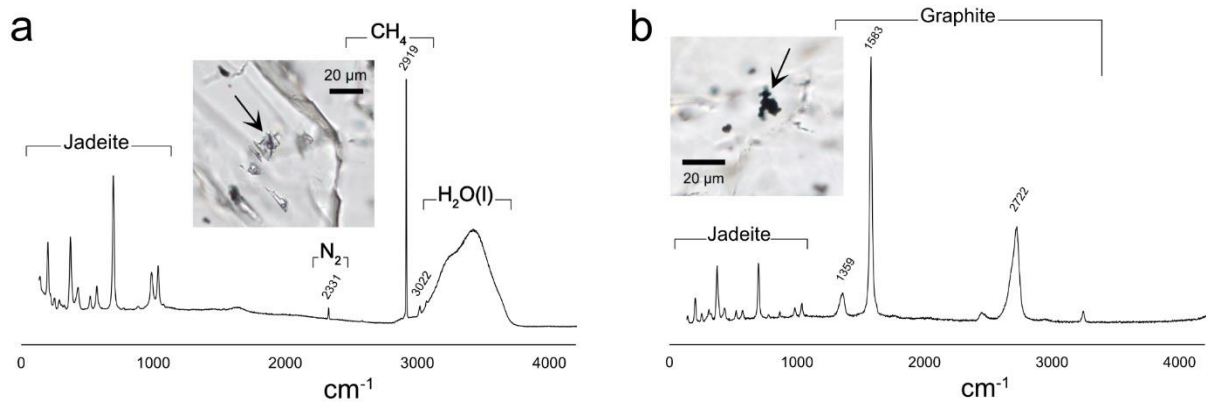


Figure S4 Raman spectra of (a) one fluid inclusion and (b) one graphite inclusion in jadeiteite sample KYJ3-2. The photomicrographs are in plane-polarized light, and they were acquired using the ZEISS ZEN core software (version 3.6).

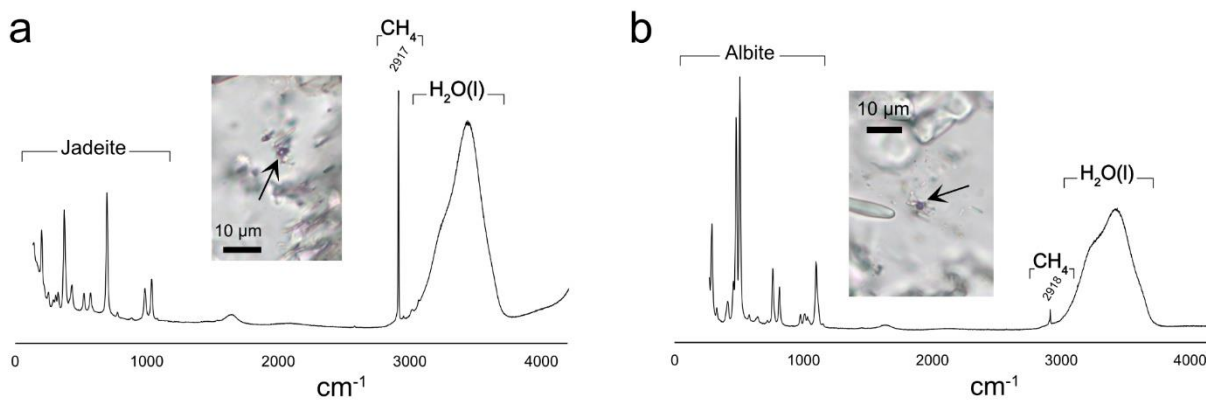


Figure S5 Raman spectra of fluid inclusions in (a) jadeite and (b) albite in jadeiteite sample KYJ3-4. The photomicrographs are in plane-polarized light, and they were acquired using the ZEISS ZEN core software (version 3.6).

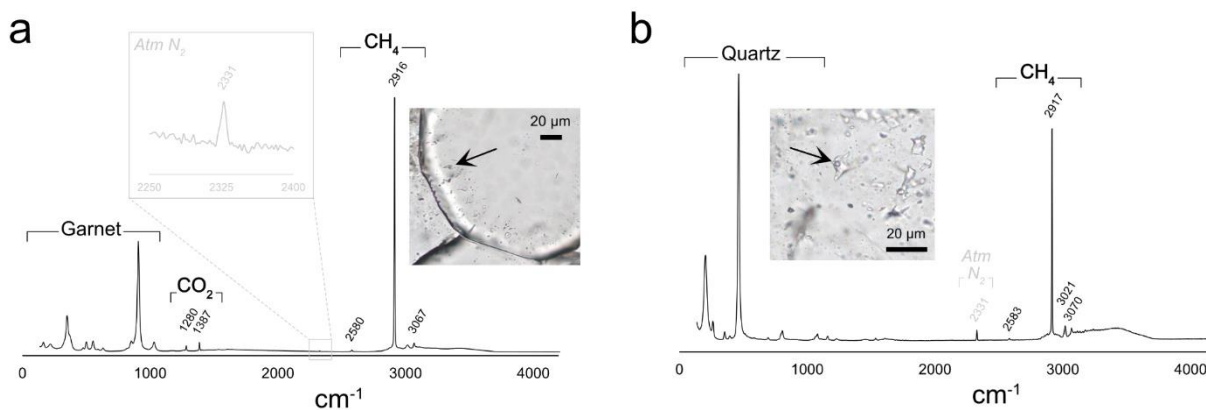


Figure S6 Raman spectra of fluid inclusions in (a) almandine-rich garnet and (b) quartz in metasomatized granite FMAB. The photomicrographs are in plane-polarized light, and they were acquired using the ZEISS ZEN core software (version 3.6). The gray boxes and text in both panels indicate uncertainty in the identification of specific chemical species.

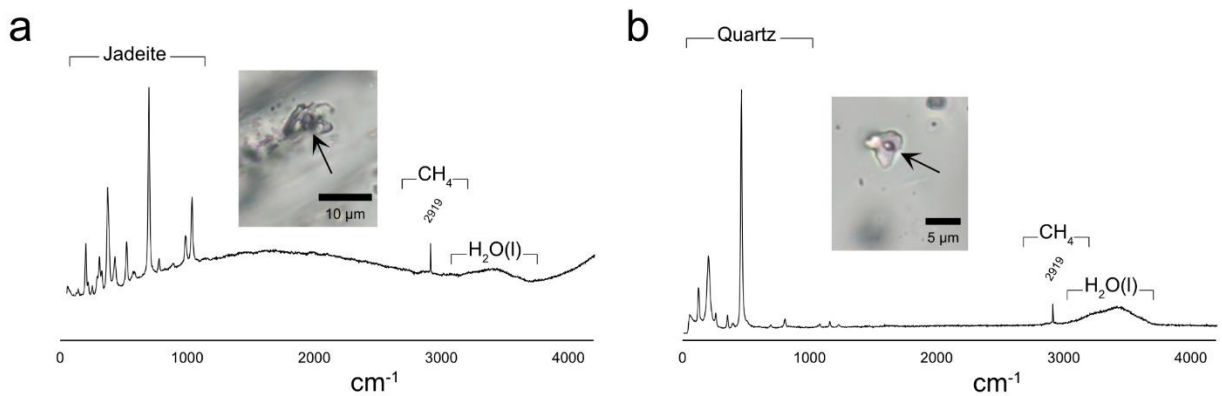


Figure S7 Raman spectra of fluid inclusions in (a) jadeite and (b) quartz in jadeite-quartz sample HKJ3. The photomicrographs are in plane-polarized light, and they were acquired using the ZEISS ZEN core software (version 3.6).

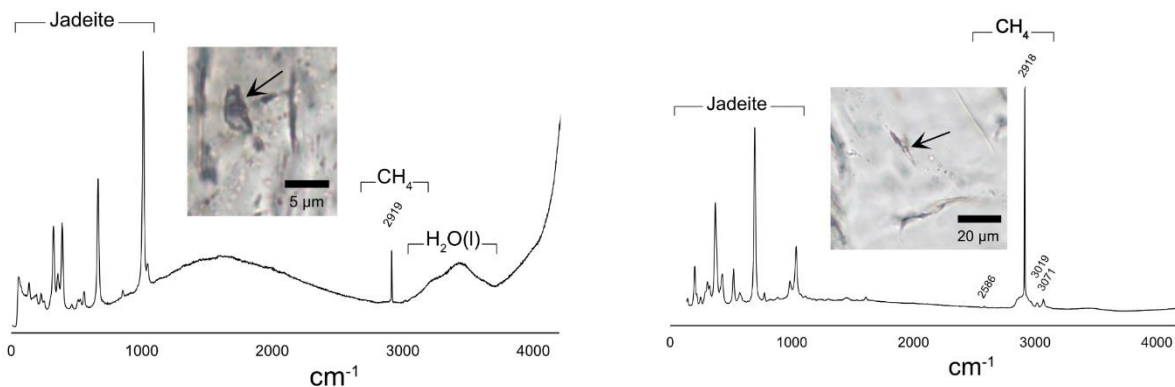


Figure S8 Raman spectrum of one fluid inclusion in diopside in diopside sample HKJ2. The photomicrograph is in plane-polarized light, and it was acquired using the ZEISS ZEN core software (version 3.6).

Figure S9 Raman spectrum of one fluid inclusion in jadeite in jadeite sample Sk3. The photomicrograph is in plane-polarized light, and it was acquired using the ZEISS ZEN core software (version 3.6).

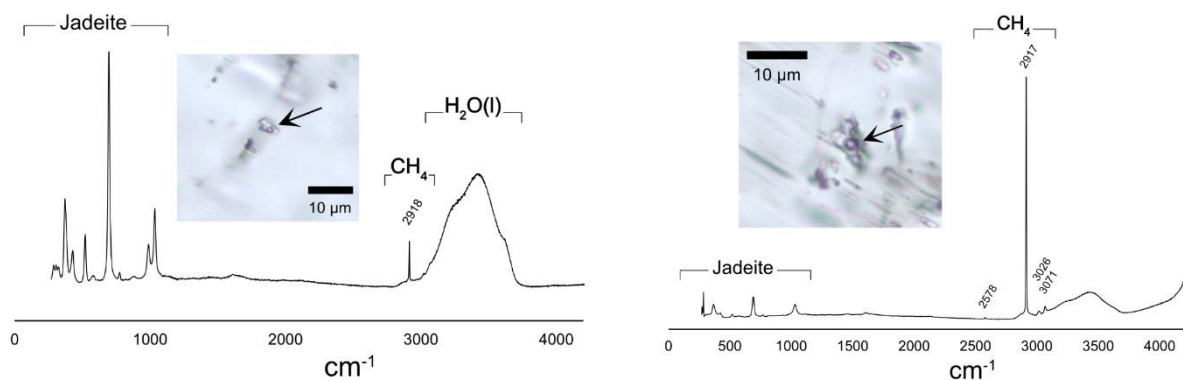


Figure S10 Raman spectrum of one fluid inclusion in jadeite in jadeite sample FI-3-MYAM. The photomicrograph is in plane-polarized light, and it was acquired using the ZEISS ZEN core software (version 3.6).

Figure S11 Raman spectrum of one fluid inclusion in jadeite in jadeite sample KZY-11. The photomicrograph is in plane-polarized light, and it was acquired using the ZEISS ZEN core software (version 3.6).

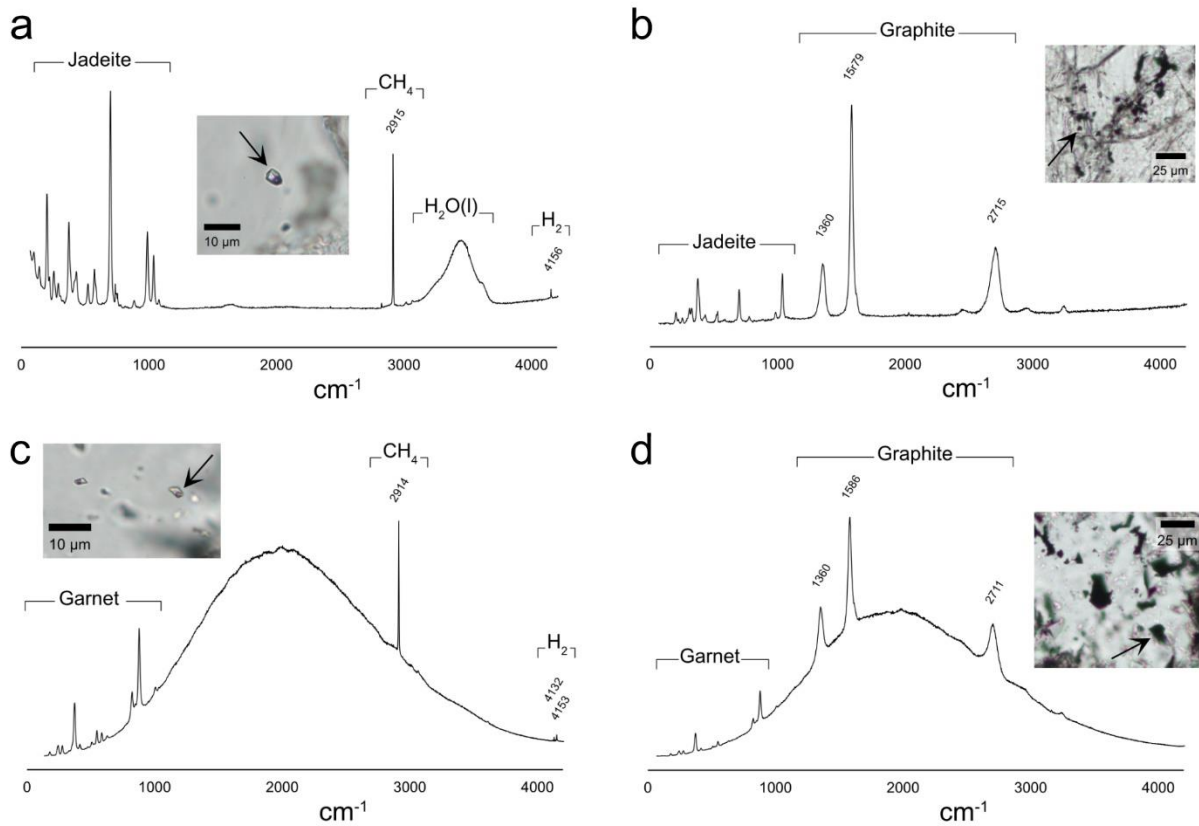


Figure S12 Raman spectra of fluid and graphite inclusions in (a–b) jadeite and (c–d) garnet in jadeitite sample 1Ba17-4e1. The photomicrographs are in plane-polarized light, and they were acquired using the ZEISS ZEN core software (version 3.6).

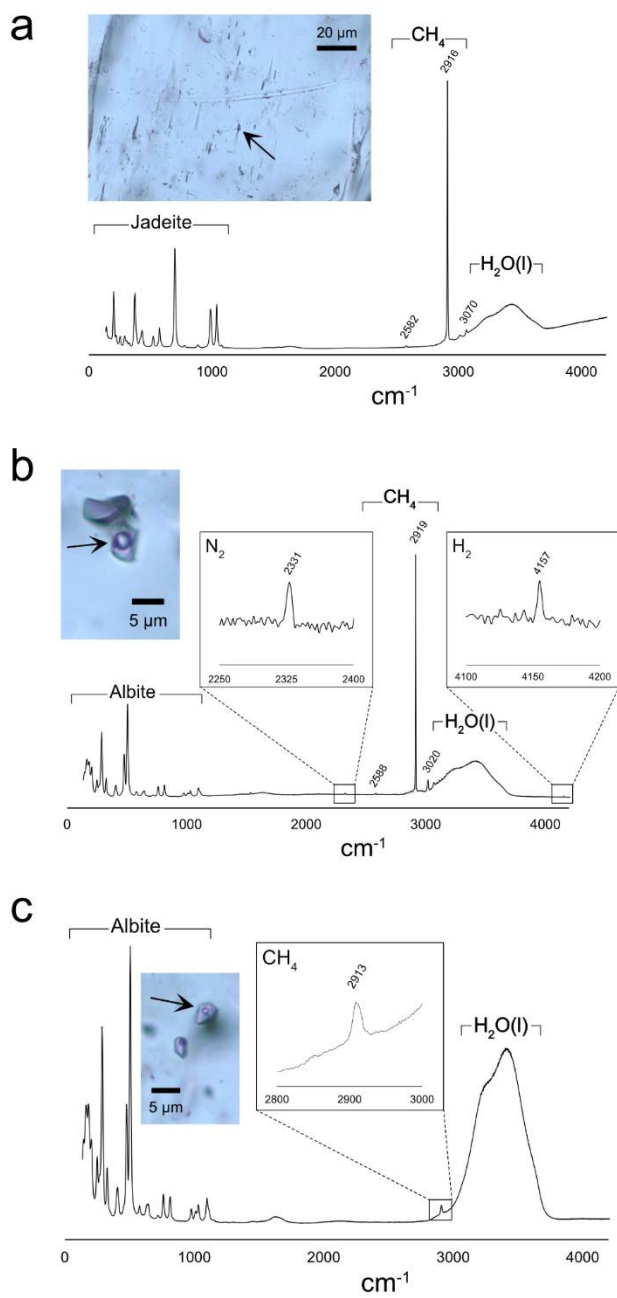


Figure S13 Raman spectra of fluid inclusions in (a) jadeite and (b–c) albite in jadeite sample Cfn1. The photomicrographs are in plane-polarized light, and they were acquired using the ZEISS ZEN core software (version 3.6).

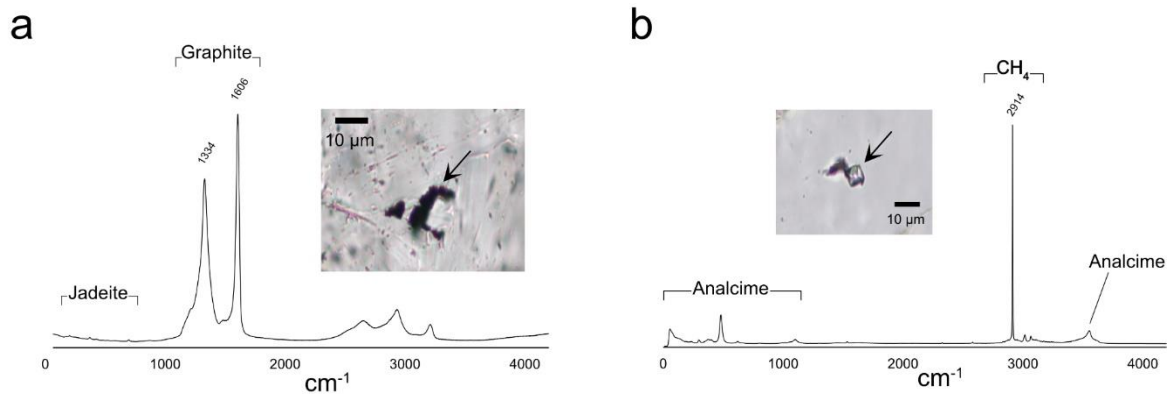


Figure S14 Raman spectra of fluid and graphite inclusions in (a) jadeite and (b) analcime in jadeitite sample N11. The photomicrographs are in plane-polarized light, and they were acquired using the ZEISS ZEN core software (version 3.6).

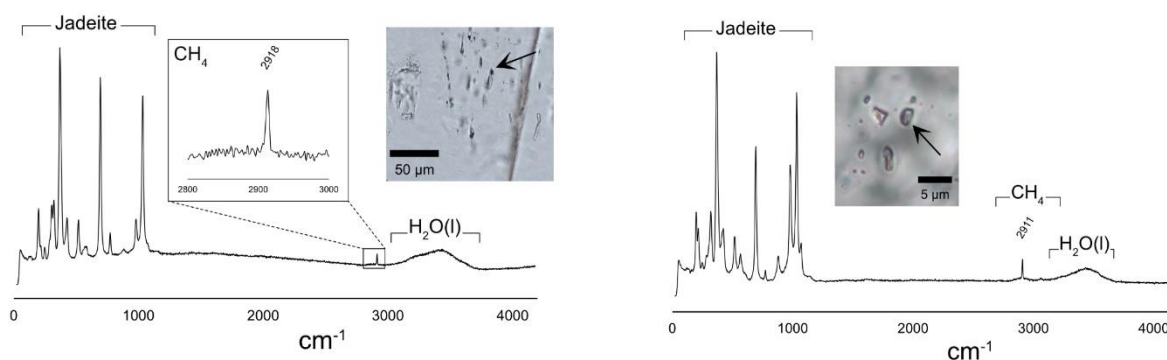


Figure S15 Raman spectrum of one fluid inclusion in jadeite in jadeitite sample SYN. The photomicrograph is in plane-polarized light, and it was acquired using the ZEISS ZEN core software (version 3.6).

Figure S16 Raman spectrum of one fluid inclusion in jadeite in jadeitite sample RSA1. The photomicrograph is in plane-polarized light, and it was acquired using the ZEISS ZEN core software (version 3.6).

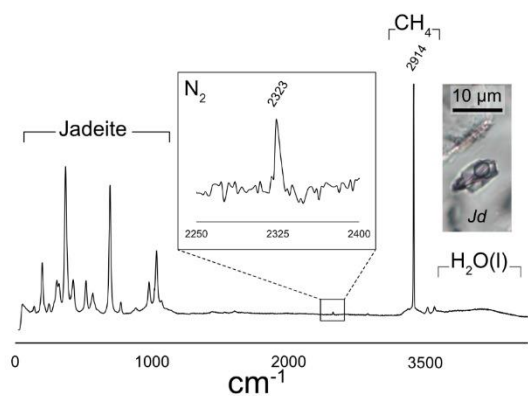


Figure S17 Raman spectrum of one fluid inclusion in jadeite in jadeitite sample PUL. The photomicrograph is in plane-polarized light, and it was acquired using the ZEISS ZEN core software (version 3.6).

Table S1 Compilation of the chemical species detected in all measured fluid inclusions in the studied sample, using the WITec alpha300 R micro-Raman spectroscope. A question mark is used to indicate uncertainty in whether fluid inclusions are primary or secondary (see Table 1), and the \pm symbol to indicate possible artifacts in the spectra.

| Country | Locality | Sample | Host | Site – Fluid inclusion # | Chemical species | Primary/secondary |
|--------------------------|--------------------------|-----------------------------------|---|---|--|-------------------|
| Guatemala | North Motagua Mélange | GT1 | Jadeite | Site 3 – FI 1 (Fig. S1a) | CH ₄ , H ₂ O, N ₂ | Primary? |
| | | | | Site 3 – FI 2 | CH ₄ , H ₂ O, N ₂ | |
| | | | Titanite | Site 1 – FI 1 | CH ₄ | Secondary |
| | | | | Site 2 – FI 2 | CH ₄ | |
| | | | Site 6 – FI 1 (Fig. S1c) | CH ₄ , H ₂ O | | |
| Japan | Osayama | OSJ1002 | Jadeite | Site 2 – FI 1 (Fig. S2a) | CH ₄ | Secondary? |
| | | | | Site 2 – FI 2 | H ₂ O | |
| | | Pectolite | Site 1 – FI 1 (Fig. S2d) | CH ₄ | Secondary | |
| | | | Site 1 – FI 2 | CH ₄ | | |
| | | R5 | Titanite | Site 1 – FI 1 (Fig. S3a) | H ₂ \pm CO ₂ \pm NH ₄ | Secondary |
| | | | | Site 1 – FI 2 | CH ₄ \pm CO ₂ | |
| | | | | Site 3 – FI 1 | CH ₄ , H ₂ | |
| | | | | Site 3 – FI 2 | CH ₄ , H ₂ | |
| | Site 6 – FI 1 (Fig. S3b) | | CH ₄ | | | |
| | Albite | | Site 6 – FI 1 | H ₂ O | | |
| | Garnet | Site 8 – FI 1 | CH ₄ , N ₂ , H ₂ O | Primary | | |
| | | Site 8 – FI 2 (Fig. S3d) | CH ₄ , N ₂ , H ₂ O | | | |
| | Apatite | Site 4 – FI 1 (Fig. S3f) | CH ₄ , H ₂ , H ₂ O | Secondary | | |
| | Itoigawa–Omi | KYJ3-2 | Jadeite | Site 1 – FI 1 | CH ₄ | Primary |
| | | | | Site 3 – FI 1 | H ₂ O, CH ₄ | |
| | | | | Site 5 – FI 1 | CH ₄ \pm H ₂ O | |
| Site 6 – FI 1 (Fig. S4a) | | | | CH ₄ , H ₂ O, N ₂ | | |
| KYJ3-4 | | Jadeite | Site 2 – FI 1 | CH ₄ , H ₂ O \pm N ₂ | Primary? | |
| | | | Site 3 – FI 1 | H ₂ O, CH ₄ | | |
| | | | Site 3 – FI 2 | H ₂ O \pm CH ₄ | | |
| | | Albite | Site 3 – FI 3 (Fig. S5a) | H ₂ O, CH ₄ | | |
| | | | Site 2 – FI 1 (Fig. S5b) | FIs: CH ₄ , H ₂ O | | |
| | | | Site 2 – FI 2 | H ₂ O \pm CH ₄ | | |
| FMAB | | Quartz | Site 2 – FI 1 | CH ₄ | Secondary? | |
| | | | Site 2 – FI 2 | H ₂ O \pm CH ₄ | | |
| | | | Site 3 – FI 1 | H ₂ O, CH ₄ | | |
| | | | Site 4 – FI 1 (Fig. S6b) | CH ₄ | | |
| | Site 6 – FI 1 | | H ₂ O, CH ₄ | | | |
| | Site 6 – FI 2 | | H ₂ O, CH ₄ | | | |
| Garnet | Site 1 – FI 1 (Fig. S6a) | CH ₄ , CO ₂ | Primary | | | |
| | Site 1 – FI 2 | CH ₄ | | | | |
| Sk3 | Jadeite | Site 4 – FI 1 (Fig. S9) | CH ₄ | Secondary | | |
| Kamuikotan (Hokkaido) | HKJ3 | Jadeite | Site 1 – FI 1 (Fig. S7a) | H ₂ O, CH ₄ | Secondary? | |
| | | | Site 4 – FI 1 | H ₂ O, CH ₄ | | |
| | Quartz | Site 2 – FI 1 | H ₂ O | Primary | | |
| | | Site 2 – FI 2 (Fig. S7b) | H ₂ O, CH ₄ | | | |
| HKJ2 | Jadeite | Site 1 – FI 1 (Fig. S8) | H ₂ O, CH ₄ | Secondary? | | |
| USA | New Idria | Cfn1 | Jadeite | Site 1 – FI 1 | CH ₄ , H ₂ O | Secondary |
| | | | | Site 2 – FI 1 | CH ₄ , H ₂ O | |
| | | | | Site 3 – FI 1 | CH ₄ , H ₂ O | |
| | | | | Site 4 – FI 1 (Fig. S13a) | CH ₄ , H ₂ O | |
| | | | | Site 4 – FI 2 | CH ₄ , H ₂ O | |
| | | | | Site 4 – FI 3 | CH ₄ , H ₂ O | |
| | | | Albite | Site 1 – FI 1 | CH ₄ , H ₂ O | Primary |

| | | | | | | |
|----------------------|-----------------|------------|----------|------------------------------------|---|-------------------|
| | | | | Site 1 – FI 2 | CH ₄ , H ₂ O | |
| | | | | Site 1 – FI 3 | CH ₄ , H ₂ O, N ₂ , H ₂ | |
| | | | | Site 7 – FI 1 (Fig. S13b) | CH ₄ , H ₂ O, N ₂ , H ₂ | |
| | | | | Site 7 – FI 2 (Fig. S13c) | CH ₄ , H ₂ O | |
| | | NII | Analcime | Site 11 – FI 1 | CH ₄ | Primary |
| Myanmar | - | FI-3-MYAM | Jadeite | Site 3 – FI 1 | CH ₄ | Pseudo-secondary? |
| | | | | Site 4 – FI 1 (Fig. S10) | CH ₄ , H ₂ O | |
| | | | | Site 8 – FI 1 | CH ₄ , H ₂ O | |
| Kazakhstan | - | KZY-11 | Jadeite | Site 6 – FI 1 | CH ₄ , H ₂ O | Secondary |
| | | | | Site 6 – FI 2 (Fig. S11) | CH ₄ , H ₂ O | |
| | | | | Site 7 – FI 1 | CH ₄ , H ₂ O | |
| Russia | Polar Urals | PUL | Jadeite | Site 1 – FI 1 | CH ₄ , H ₂ O, N ₂ | Secondary? |
| | | | | Site 3 – FI 1 (Fig. S17) | CH ₄ , H ₂ O, N ₂ | Secondary |
| | | | | Site 4 – FI 1 | CH ₄ , H ₂ O | |
| | Chukotka | RSA1 | Jadeite | Site 4 – FI 1 (Fig. S16) | H ₂ O, CH ₄ | Primary |
| | West Sayan | SYN | Jadeite | Site 1 – FI 1 | H ₂ O, CH ₄ | Primary |
| | | | | Site 2 – FI 1 (Fig. S15) | H ₂ O, CH ₄ | |
| Site 3 – FI 1 | | | | CH ₄ ± H ₂ O | | |
| Western Alps (Italy) | Lanzo Massif | 1Bal17-4e1 | Jadeite | Site 1 – FI 1 | CH ₄ , H ₂ O | Primary |
| | | | | Site 2 – FI 1 (Fig. S12a) | CH ₄ , H ₂ O, H ₂ | |
| | | | | Site 3 – FI 1 | CH ₄ , H ₂ O | |
| | | | | Site 4 – FI 1 | H ₂ O | |
| | | | Garnet | Site 1 – FI 1 (Fig. S12c) | CH ₄ , H ₂ | Primary |
| | | | | Site 2 – FI 1 | CH ₄ | |
| | | | | Site 4 – FI 1 | CH ₄ , H ₂ | |
| | | | | Site 4 – FI 2 | CH ₄ , H ₂ | |
| | | | | Site 5 – FI 1 | CH ₄ , H ₂ | |
| | | | | Site 6 – FI 1 | CH ₄ | |
| Site 7 – FI 1 | CH ₄ | | | | | |

A2. Titanite U–Pb geochronology by laser ablation inductively coupled plasma mass spectrometry

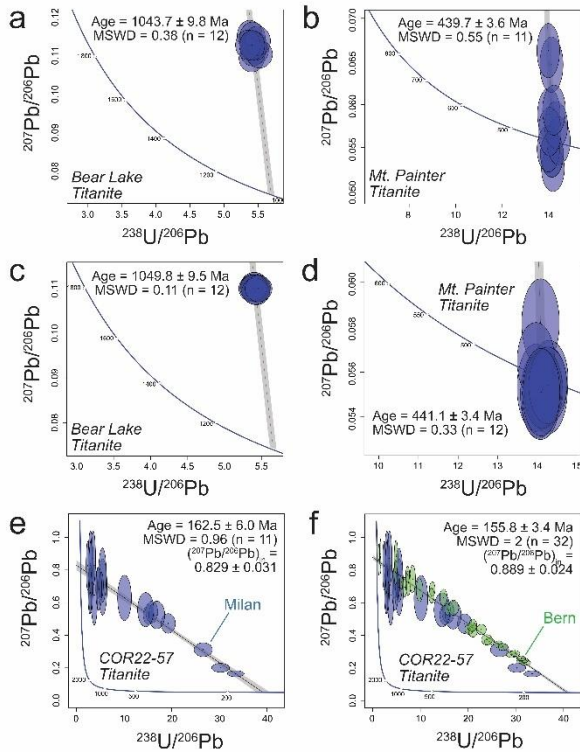


Figure S18 Tera–Wasserburg plots of titanite reference materials (a) Bear Lake and (b) Mt. Painters measured during our first analytical session at the University of Milan (Italy), (c) Bear Lake and (d) Mt. Painter during our second session at the University of Milan, and in-house titanite reference material COR22-57 measured at the University of Milan (e) and at the University of Bern (f; Switzerland). A and C are anchored to an initial $^{207}\text{Pb}/^{206}\text{Pb}$ value of 0.916 ± 0.050 (Ma et al., 2019), while (b) and (d) to an initial $^{207}\text{Pb}/^{206}\text{Pb}$ value of 0.87 ± 0.05 (Elburg et al., 2003); (e–f) are not anchored to an initial $^{207}\text{Pb}/^{206}\text{Pb}$ value. Error ellipses are 2σ and age uncertainties are at 95 % confidence level. Plotted using IsoplotR (Vermeesch, 2018).

during both analytical sessions. During these sessions, titanite in jadeitite samples GT-1, OSJ1002 and R5 were analyzed (Table S5).

A third analytical session was carried out at the University of Bern, Switzerland, to try to better constrain the age of sample GT1. Because no well-characterized titanite standard was available at the time at the University of Bern, we used titanite sample COR22-57 as in-house standard (Table S3). During the first analytical session at ESD-UniMi, COR22-57 titanite returned an age of 162.5 ± 6.0 Ma (MSWD = 0.96; $n = 21$; initial $^{207}\text{Pb}/^{206}\text{Pb}$ ratio = 0.829 ± 0.031 ; Fig. S18e). During the third analytical session at the University of Bern, titanite sample COR22-57 gave an age of 155.8 ± 3.4 (MSWD = 2; $n = 32$; initial $^{207}\text{Pb}/^{206}\text{Pb}$ ratio = 0.888 ± 0.016 ; Fig. S18f) in a Tera–

Measurement conditions at University of Milan (ESD-UniMi) and at the University of Bern are given in Tables S2 and S3, respectively. All Tera–Wasserburg diagrams are plotted using IsoplotR (Vermeesch, 2018).

In the first measurement session at ESD-UniMi, Bear Lake and Mt. Painter titanite secondary reference materials (Fig. S18a–b) gave ages of, respectively, 1043.7 ± 9.8 Ma (MSWD = 0.38; $n = 12$) and 439.7 ± 3.6 Ma (MSWD = 0.55; $n = 11$) in anchored Tera–Wasserburg plots (see Table S4 for isotopic ratios). In the second session at the ESD-UniMi, Bear Lake (Ma et al., 2019) and Mt. Painter (Elburg et al., 2003) titanite secondary reference materials (Fig. S18c–d) gave ages of, respectively, 1049.8 ± 9.5 Ma (MSWD = 0.11; $n = 12$) and 441.1 ± 3.4 Ma (MSWD = 0.33; $n = 12$) in anchored Tera–Wasserburg diagrams. These dates are within uncertainty of the reference ages of these reference materials, attesting to robust and accurate U–Pb isotope ratio being measured

Wasserburg diagram (Fig. S18f), consistent with the age obtained at ESD-UniMi, attesting to good analytical conditions and to the reliability of the measured U–Pb isotope data. Titanite in jadeitite GT-1 returned $^{207}\text{Pb}/^{206}\text{Pb}$ ratio with propagated 2 S.E. of 2–10 % and only one measurement with propagated 2 S.E. > 6 % (Table S4). Titanite GT-1 gave an age of 71.8 ± 4.0 Ma (MSWD = 1.4; $n = 27$; initial $^{207}\text{Pb}/^{206}\text{Pb}$ ratio = 0.841 ± 0.007 ; Fig. 3a). If we plot the dataset obtained at ESD-UniMi with that obtained at the University of Bern in one Tera–Wasserburg diagram, the combined dataset gives an age of 71.3 ± 5.3 Ma (MSWD = 1.7; $n = 49$; initial $^{207}\text{Pb}/^{206}\text{Pb}$ ratio = 0.8366 ± 0.0087). Because the MSWD value resulting from plotting both datasets together is reasonably low (i.e., consistent with only one titanite generation resolvable at the available analytical precision), and both age and initial $^{207}\text{Pb}/^{206}\text{Pb}$ ratio remain consistent with the individual Tera–Wasserburg data, and because our in-house reference material COR22-57 gave the same age within uncertainty between the analytical sessions performed at both laboratories, we conclude that the more precise age of 71.8 ± 4.0 Ma (MSWD = 1.4; $n = 27$; initial $^{207}\text{Pb}/^{206}\text{Pb}$ ratio = 0.841 ± 0.007 ; Fig. 3a) obtained at the University of Bern can be considered reliable to date titanite in jadeitite GT-1, and only this age is discussed in the main text.

| Table S2. Measurement conditions for U–Pb isotope data in titanite by LA-ICP-MS at ESD-UniMi. | |
|--|---|
| Laboratory & Sample Preparation | |
| Laboratory name | Geochemistry, Geochronology and Isotope Geology laboratory hosted at the Earth Sciences Department of the University of Milan (Italy) |
| Sample type/mineral | Titanite |
| Sample preparation | Thin sections |
| Imaging | Backscattered electron imaging: 1 nA beam current, 20 kV acceleration voltage, working distances of 8.5 mm |
| Laser ablation system | |
| Make, Model & type | 193nm ATLEX 300 LR ultra-short pulse, compact, air-cooled excimer laser (Analyte Excite+ from Teledyne Photon Machines) |
| Ablation cell & volume | Double volume cell - HelEx II |
| Laser wavelength | 193 nm |
| Pulse width | < 5 nsec |
| On-sample fluence | 3 J cm ⁻² (first session) and 4 J cm ⁻² (second session) |
| Repetition rate | 10 Hz |
| Ablation duration | 40 sec (first session) and 40 sec (second session) |
| Spot diameter | 50 μm |
| Sampling mode | Static spot ablation |
| Carrier gas | He (0.5 l min ⁻¹ in the cell and 0.3 l min ⁻¹ in the arm) mixed with Ar prior to introduction to ICP |
| ICP-MS Instrument | |
| Make, Model & type | Single-detector quadrupole ICP-MS iCAP RQ from Thermo Fisher Scientific |
| Sample introduction | Ablation aerosol |
| RF power | 1550 W |
| Sampler, skimmer cones | Ni |
| Detection system | Single collector secondary electron multiplier |
| Data acquisition protocol | Time-resolved analysis |
| Scanning mode | Peak-hopping one point per peak |
| Detector mode | Pulse counting, dead time correction applied and analog mode when signal intensity > 10 ⁶ cps |
| Masses measured | 206, 207, 208, 232, 238 |
| Dwell times | 40 msec (206, 207, 238), 20 msec (208, 232) |
| Sweep time | ca. 0.16 sec |

| | |
|--|---|
| Th/U (232/238) ratios and oxide production (248/232) | 1.0 and < 0.5 % measured on NIST 612 using a beam size 40 μm , fluence 6 J cm^{-2} , repetition rate 5 Hz, scan rate 10 $\mu\text{m sec}^{-1}$ (first session); 1.2 and < 0.4 % measured on NIST 612 using a beam size 40 μm , fluence 7 J cm^{-2} , repetition rate 5 Hz, scan rate 10 $\mu\text{m sec}^{-1}$ (second session) |
| Sensitivity on mass 232 | 3600 cps ppm^{-1} measured on NIST 612 using a beam size 40 μm , fluence 6 J cm^{-2} , repetition rate 5 Hz, scan rate 5 $\mu\text{m sec}^{-1}$ (first session); 3700 cps ppm^{-1} measured on NIST 612 using a beam size 40 μm , fluence 7 J cm^{-2} , repetition rate 5 Hz, scan rate 5 $\mu\text{m sec}^{-1}$ (second session) |
| IC Dead time | 40 nsec |
| Data Processing | |
| Gas blank | 30 sec on-peak zero subtracted |
| Calibration strategy | MKED1 titanite used as primary reference material |
| Primary reference material | MKED1 titanite (Spandler et al., 2016) (^{207}Pb -correction using an initial $^{207}\text{Pb}/^{206}\text{Pb}$ ratio of 0.95) |
| Data processing package | Glitter (Griffin et al., 2008) |
| Initial Pb correction | No initial Pb correction applied to titanite unknowns and secondary reference materials |
| Uncertainty level & propagation | Age uncertainties are 2 standard errors (2 S.E.) without propagation of the long-term reproducibility of titanite secondary reference materials |
| Quality control / Validation | Bear Lake (Ma et al., 2019) and Mt. Painter (Elburg et al., 2003) |
| Other information | - |

Table S3. Measurement conditions for U–Pb isotope data in titanite by LA-ICP-MS at the University of Bern.

| | |
|--|--|
| Laboratory & Sample Preparation | |
| Laboratory name | Institute of Geological Sciences, University of Bern (Switzerland) |
| Sample type/mineral | Titanite |
| Sample preparation | Thin sections |
| Imaging | Backscattered electron imaging: 1 nA beam current, 20 kV acceleration voltage, working distances of 8.5 mm |
| Laser ablation system | |
| Make, Model & type | Resonetics RESOLutionSE 193 nm excimer laser |
| Ablation cell & volume | S-155 large volume constant geometry cell (Laurin Technic, Australia) |
| Laser wavelength | 193 nm |
| Pulse width | 5 nsec |
| On-sample fluence | 4 J cm^{-2} |
| Repetition rate | 5 Hz |
| Ablation duration | 30 sec |
| Spot diameter | 50 μm |
| Sampling mode | Static spot ablation |
| Carrier gas | Pure He (0.4 l min^{-1}) and N_2 (0.003 l min^{-1}) mixed with Ar (0.86 l min^{-1}) immediately after the ablation cell |
| Cell carrier gas flow | 0.86 l min^{-1} |
| ICP-MS Instrument | |
| Make, Model & type | Agilent 7900 single quadrupole |
| Sample introduction | Ablation aerosol with squid device |
| RF power | 1400 W |
| Sampler, skimmer cones | Ni |
| Detection system | Single collector secondary electron multiplier |
| Data acquisition protocol | Time-resolved analysis |
| Scanning mode | Peak-hopping one point per peak |
| Detector mode | Pulse counting, dead time correction applied and analog mode when signal intensity > 10^6 cps |
| Masses measured | 206, 207, 208, 232, 238 |
| Dwell times | 40 msec (masses 206, 207, 208, 238) and 20 msec (mass 232) |
| Sweep time | ca. 0.21 sec |
| Th/U (232/238) ratios and oxide production (248/232) | > 98 % and < 0.2 %; measured on NIST 612 with beam size 50 μm , fluence 2.5 J cm^{-2} , repetition rate 5 Hz, scan rate 5 $\mu\text{m sec}^{-1}$ |
| Sensitivity on mass 232 | 7390 cps ppm^{-1} measured on NIST 612 using a beam size 50 μm , fluence 2.5 J cm^{-2} , repetition rate 5 Hz, scan rate 5 $\mu\text{m sec}^{-1}$ |
| IC Dead time | 38 nsec |
| Data Processing | |
| Gas blank | 30 sec on-peak zero subtracted |
| Calibration strategy | MKED1 titanite used as primary reference material |
| Primary reference material | MKED1 titanite (Spandler et al., 2016) (^{207}Pb -correction using an initial $^{207}\text{Pb}/^{206}\text{Pb}$ ratio of 0.95) |
| Data processing package | Iolite 7.08 and the VizualAge_UcomPbine Data Reduction Scheme (Chew et al., 2014) |
| Initial Pb correction | No initial Pb correction applied to titanite unknowns and secondary reference materials |

| | |
|---------------------------------|---|
| Uncertainty level & propagation | Age uncertainties are 2 standard errors (2 S.E.) without propagation of the long-term reproducibility of titanite secondary reference materials |
| Quality control / Validation | Own titanite sample (COR22-57) used as in-house secondary reference material |
| Other information | - |

Table S4. U–Pb isotope ratios of titanite secondary reference materials used for quality control. Subscript "in": initial; subscript "rad": radiogenic. First and second sessions at the University of Milan (Italy); third session at the University of Bern (Switzerland).

| Spot | f_{206} | $^{238}\text{U}/^{206}\text{U}$ | 2 S.E. | $^{207}\text{Pb}/^{206}\text{Pb}$ | 2 S.E. | $^{207}\text{Pb}/^{235}\text{U}$ | 2 S.E. | $^{206}\text{Pb}/^{238}\text{U}$ | 2 S.E. | rho | $(^{207}\text{Pb}/^{206}\text{Pb})_{\text{in}}$ | $(^{207}\text{Pb}/^{206}\text{Pb})_{\text{rad}}$ |
|------------------------------------|-----------|---------------------------------|--------|-----------------------------------|---------|----------------------------------|---------|----------------------------------|---------|---------|---|--|
| Bear Lake titanite (first session) | | | | | | | | | | | | |
| 1 | 0.04 | 5.4669 | 0.1512 | 0.1117 | 0.0029 | 2.8374 | 0.0894 | 0.18292 | 0.00506 | 0.87755 | 0.916 | 0.07435 |
| 2 | 0.04 | 5.4031 | 0.1506 | 0.1096 | 0.0029 | 2.8146 | 0.0899 | 0.18508 | 0.00516 | 0.87266 | | |
| 3 | 0.05 | 5.38 | 0.15 | 0.11551 | 0.00326 | 2.96 | 0.10 | 0.186 | 0.005 | 0.830 | | |
| 4 | 0.05 | 5.4159 | 0.1519 | 0.11506 | 0.00326 | 2.9249 | 0.0991 | 0.18464 | 0.00518 | 0.82784 | | |
| 5 | 0.05 | 5.4192 | 0.1515 | 0.11319 | 0.00302 | 2.8921 | 0.0933 | 0.18453 | 0.00516 | 0.86717 | | |
| 6 | 0.05 | 5.420 | 0.150 | 0.113 | 0.003 | 2.887 | 0.092 | 0.1845 | 0.0051 | 0.8675 | | |
| 7 | 0.04 | 5.4198 | 0.1504 | 0.11126 | 0.00296 | 2.8415 | 0.0912 | 0.18451 | 0.00512 | 0.86419 | | |
| 8 | 0.04 | 5.5209 | 0.1536 | 0.11069 | 0.00294 | 2.7747 | 0.0894 | 0.18113 | 0.00504 | 0.86399 | | |
| 9 | 0.05 | 5.4448 | 0.1524 | 0.11281 | 0.00308 | 2.8606 | 0.0942 | 0.18366 | 0.00514 | 0.84970 | | |
| 10 | 0.05 | 5.491 | 0.154 | 0.11415 | 0.00312 | 2.871 | 0.095 | 0.1821 | 0.0051 | 0.8497 | | |
| 11 | 0.05 | 5.350 | 0.150 | 0.1131 | 0.0032 | 2.915 | 0.098 | 0.1869 | 0.0052 | 0.8378 | | |
| 12 | 0.05 | 5.4095 | 0.1516 | 0.11298 | 0.00316 | 2.8802 | 0.0965 | 0.18486 | 0.00518 | 0.83652 | | |
| Mount Painter (first session) | | | | | | | | | | | | |
| 1 | 0.00 | 14.1 | 0.4 | 0.0542 | 0.0022 | 0.533 | 0.023 | 0.071 | 0.002 | 0.643 | 0.87 | 0.05571 |
| 2 | 0.00 | 14.2 | 0.4 | 0.05252 | 0.00214 | 0.514 | 0.023 | 0.071 | 0.002 | 0.642 | | |
| 3 | 0.00 | 14.01 | 0.40 | 0.05886 | 0.00246 | 0.5781 | 0.0262 | 0.0714 | 0.0020 | 0.6314 | | |
| 4 | 0.01 | 14.12 | 0.41 | 0.06461 | 0.00264 | 0.63048 | 0.02796 | 0.07084 | 0.00204 | 0.64936 | | |
| 5 | 0.00 | 14.1 | 0.4 | 0.05422 | 0.00216 | 0.531 | 0.023 | 0.071 | 0.002 | 0.649 | | |
| 6 | 0.00 | 13.99 | 0.40 | 0.0549 | 0.0022 | 0.5421 | 0.0237 | 0.0715 | 0.0020 | 0.6537 | | |
| 7 | 0.01 | 13.980 | 0.399 | 0.06625 | 0.00258 | 0.65401 | 0.02786 | 0.07153 | 0.00204 | 0.66949 | | |
| 8 | 0.00 | 14.420 | 0.412 | 0.0558 | 0.0023 | 0.53403 | 0.02370 | 0.06935 | 0.00198 | 0.64333 | | |
| 9 | 0.00 | 14.314 | 0.406 | 0.0576 | 0.0023 | 0.55535 | 0.02392 | 0.06986 | 0.00198 | 0.65802 | | |
| 10 | 0.00 | 14.0 | 0.402 | 0.05686 | 0.00232 | 0.55795 | 0.02478 | 0.07122 | 0.00204 | 0.64494 | | |
| 11 | 0.00 | 14.2 | 0.4 | 0.05934 | 0.00238 | 0.575 | 0.025 | 0.070 | 0.002 | 0.649 | | |
| Sample COR22-57 (first session) | | | | | | | | | | | | |
| 1 | 0.86 | 4.546 | 0.362 | 0.71936 | 0.07942 | 21.90 | 2.01 | 0.2200 | 0.0175 | 0.8687 | 0.829 | 0.04934 |
| 2 | 0.15 | 33.44 | 1.43 | 0.1643 | 0.0154 | 0.6794 | 0.0610 | 0.0299 | 0.0013 | 0.4767 | | |
| 3 | 0.77 | 3.7597 | 0.5581 | 0.6460 | 0.1498 | 23.707 | 4.662 | 0.26598 | 0.03948 | 0.75482 | | |
| 4 | 0.83 | 5.515 | 0.745 | 0.6958 | 0.1414 | 17.43 | 2.90 | 0.1813 | 0.0245 | 0.8124 | | |
| 5 | 0.92 | 5.46 | 0.67 | 0.76851 | 0.13588 | 19.4 | 2.8 | 0.183 | 0.022 | 0.862 | | |
| 6 | 0.34 | 26.617 | 1.573 | 0.31153 | 0.03494 | 1.6166 | 0.1646 | 0.03757 | 0.00222 | 0.58047 | | |
| 7 | 1.01 | 2.966 | 0.425 | 0.83693 | 0.16538 | 38.93 | 6.34 | 0.3372 | 0.0483 | 0.8802 | | |
| 8 | 0.81 | 3.0151 | 0.3626 | 0.68225 | 0.12074 | 31.245 | 4.705 | 0.33166 | 0.03988 | 0.79858 | | |
| 9 | 0.80 | 2.841 | 0.337 | 0.6711 | 0.1145 | 32.611 | 4.726 | 0.3519 | 0.0417 | 0.8177 | | |

| | | | | | | | | | | | | |
|----|------|--------|--------|---------|---------|---------|---------|---------|---------|---------|--|--|
| 10 | 1.00 | 2.3662 | 0.2633 | 0.82605 | 0.12116 | 48.191 | 5.937 | 0.42262 | 0.04702 | 0.90310 | | |
| 11 | 0.98 | 3.119 | 0.395 | 0.8153 | 0.1395 | 36.09 | 5.03 | 0.3206 | 0.0406 | 0.9090 | | |
| 12 | 0.84 | 5.2422 | 0.3430 | 0.70784 | 0.06406 | 18.644 | 1.425 | 0.19076 | 0.01248 | 0.85592 | | |
| 13 | 0.61 | 15.168 | 0.9156 | 0.52548 | 0.04964 | 4.7818 | 0.3892 | 0.06593 | 0.00398 | 0.74175 | | |
| 14 | 0.19 | 30.239 | 1.5179 | 0.20059 | 0.02232 | 0.91508 | 0.09628 | 0.03307 | 0.00166 | 0.47709 | | |
| 15 | 0.81 | 4.6979 | 0.5134 | 0.68466 | 0.10816 | 20.168 | 2.609 | 0.21286 | 0.02326 | 0.84475 | | |
| 16 | 1.05 | 3.515 | 0.418 | 0.87164 | 0.13736 | 34.23 | 4.30 | 0.2845 | 0.0338 | 0.9461 | | |
| 17 | 0.74 | 10.094 | 1.188 | 0.6285 | 0.1142 | 8.5878 | 1.2744 | 0.09907 | 0.01166 | 0.7931 | | |
| 18 | 0.54 | 19.26 | 1.22 | 0.47214 | 0.04946 | 3.390 | 0.308 | 0.0519 | 0.0033 | 0.6986 | | |
| 19 | 0.63 | 15.810 | 1.035 | 0.5422 | 0.0546 | 4.74159 | 0.40414 | 0.06325 | 0.00414 | 0.7679 | | |
| 20 | 0.61 | 16.9 | 1.4 | 0.52414 | 0.06958 | 4.292 | 0.481 | 0.059 | 0.005 | 0.726 | | |
| 21 | 0.65 | 14.53 | 1.39 | 0.55675 | 0.08588 | 5.284 | 0.681 | 0.0688 | 0.0066 | 0.7402 | | |

Bear Lake titanite (second session)

| | | | | | | | | | | | | |
|----|------|------|------|--------|--------|------|------|-------|-------|-------|-------|---------|
| 1 | 0.04 | 5.40 | 0.15 | 0.1107 | 0.0024 | 2.82 | 0.08 | 0.185 | 0.005 | 0.970 | 0.916 | 0.07435 |
| 2 | 0.04 | 5.37 | 0.15 | 0.1100 | 0.0024 | 2.82 | 0.08 | 0.186 | 0.005 | 0.971 | | |
| 3 | 0.04 | 5.44 | 0.15 | 0.1102 | 0.0023 | 2.79 | 0.08 | 0.184 | 0.005 | 0.988 | | |
| 4 | 0.04 | 5.43 | 0.15 | 0.1099 | 0.0023 | 2.79 | 0.08 | 0.184 | 0.005 | 0.988 | | |
| 5 | 0.04 | 5.41 | 0.15 | 0.1101 | 0.0024 | 2.80 | 0.08 | 0.185 | 0.005 | 0.974 | | |
| 6 | 0.04 | 5.43 | 0.15 | 0.1093 | 0.0024 | 2.78 | 0.08 | 0.184 | 0.005 | 0.972 | | |
| 7 | 0.04 | 5.43 | 0.15 | 0.1100 | 0.0024 | 2.79 | 0.08 | 0.184 | 0.005 | 0.972 | | |
| 8 | 0.04 | 5.40 | 0.15 | 0.1104 | 0.0024 | 2.82 | 0.08 | 0.185 | 0.005 | 0.970 | | |
| 9 | 0.04 | 5.40 | 0.15 | 0.1102 | 0.0024 | 2.81 | 0.08 | 0.185 | 0.005 | 0.970 | | |
| 10 | 0.04 | 5.39 | 0.15 | 0.1101 | 0.0024 | 2.82 | 0.08 | 0.185 | 0.005 | 0.967 | | |
| 11 | 0.04 | 5.41 | 0.15 | 0.1094 | 0.0024 | 2.79 | 0.08 | 0.185 | 0.005 | 0.966 | | |
| 12 | 0.04 | 5.46 | 0.15 | 0.1100 | 0.0024 | 2.78 | 0.08 | 0.183 | 0.005 | 0.965 | | |

Mount Painter (second session)

| | | | | | | | | | | | | |
|----|------|-------|------|--------|--------|--------|--------|--------|--------|--------|------|---------|
| 1 | 0.00 | 14.04 | 0.39 | 0.0550 | 0.0015 | 0.5404 | 0.0176 | 0.0712 | 0.0020 | 0.8431 | 0.87 | 0.05571 |
| 2 | 0.00 | 14.27 | 0.40 | 0.0553 | 0.0015 | 0.5465 | 0.0178 | 0.0716 | 0.0020 | 0.8485 | | |
| 3 | 0.00 | 13.96 | 0.39 | 0.0582 | 0.0015 | 0.5699 | 0.0181 | 0.0710 | 0.0020 | 0.8696 | | |
| 4 | 0.00 | 14.08 | 0.39 | 0.0557 | 0.0015 | 0.5371 | 0.0171 | 0.0700 | 0.0019 | 0.8599 | | |
| 5 | 0.00 | 14.29 | 0.39 | 0.0552 | 0.0015 | 0.5378 | 0.0171 | 0.0706 | 0.0019 | 0.8662 | | |
| 6 | 0.00 | 14.16 | 0.39 | 0.0553 | 0.0014 | 0.5391 | 0.0171 | 0.0707 | 0.0019 | 0.8673 | | |
| 7 | 0.00 | 14.15 | 0.39 | 0.0565 | 0.0015 | 0.5581 | 0.0176 | 0.0716 | 0.0020 | 0.8755 | | |
| 8 | 0.00 | 13.96 | 0.39 | 0.0547 | 0.0014 | 0.5360 | 0.0171 | 0.0710 | 0.0020 | 0.8658 | | |
| 9 | 0.00 | 14.08 | 0.39 | 0.0552 | 0.0015 | 0.5394 | 0.0173 | 0.0708 | 0.0019 | 0.8531 | | |
| 10 | 0.00 | 14.12 | 0.39 | 0.0552 | 0.0015 | 0.5337 | 0.0173 | 0.0701 | 0.0019 | 0.8550 | | |
| 11 | 0.00 | 14.26 | 0.39 | 0.0554 | 0.0015 | 0.5355 | 0.0172 | 0.0701 | 0.0019 | 0.8624 | | |
| 12 | 0.00 | 14.09 | 0.39 | 0.0551 | 0.0015 | 0.5391 | 0.0175 | 0.0710 | 0.0019 | 0.8412 | | |

Sample COR22-57 (third session)

| | | | | | | | | | | | | |
|---|------|-------|-------|-------|-------|-------|------|--------|--------|--------|-------|---------|
| 1 | 0.61 | 15.7 | 0.5 | 0.56 | 0.03 | 4.9 | 0.22 | 0.064 | 0.002 | 0.698 | 0.889 | 0.04919 |
| 2 | 0.83 | 8.35 | 0.49 | 0.75 | 0.07 | 11.63 | 0.76 | 0.120 | 0.007 | 0.895 | | |
| 3 | 0.81 | 5.970 | 0.264 | 0.726 | 0.034 | 16.7 | 0.86 | 0.1675 | 0.0074 | 0.8579 | | |
| 4 | 0.77 | 6.698 | 0.350 | 0.696 | 0.049 | 13.67 | 0.81 | 0.1493 | 0.0078 | 0.8817 | | |
| 5 | 0.46 | 20.20 | 0.73 | 0.438 | 0.026 | 2.97 | 0.15 | 0.0495 | 0.0018 | 0.7200 | | |

| | | | | | | | | | | |
|----|------|--------|--------|-------|-------|-------|-------|---------|---------|---------|
| 6 | 0.22 | 32.00 | 0.92 | 0.233 | 0.013 | 0.988 | 0.051 | 0.0313 | 0.0009 | 0.5579 |
| 7 | 0.28 | 29.10 | 0.93 | 0.284 | 0.016 | 1.327 | 0.069 | 0.0344 | 0.0011 | 0.6155 |
| 8 | 0.80 | 7.43 | 0.44 | 0.72 | 0.06 | 12.73 | 0.92 | 0.135 | 0.008 | 0.823 |
| 9 | 1.08 | 0.9200 | 0.0635 | 0.952 | 0.079 | 136 | 11 | 1.087 | 0.075 | 0.853 |
| 10 | 0.88 | 4.78 | 0.25 | 0.787 | 0.062 | 21.9 | 1.4 | 0.209 | 0.011 | 0.823 |
| 11 | 1.01 | 1.6 | 0.1 | 0.9 | 0.1 | 73.3 | 5.7 | 0.63 | 0.05 | 0.94 |
| 12 | 0.99 | 4.88 | 0.31 | 0.882 | 0.083 | 22.3 | 1.4 | 0.205 | 0.013 | 1.010 |
| 13 | 0.62 | 16.92 | 0.89 | 0.57 | 0.04 | 4.56 | 0.32 | 0.0591 | 0.0031 | 0.7475 |
| 14 | 0.71 | 12.33 | 0.47 | 0.644 | 0.037 | 7.02 | 0.36 | 0.0811 | 0.0031 | 0.7454 |
| 15 | 0.45 | 21.01 | 0.75 | 0.425 | 0.029 | 2.72 | 0.16 | 0.0476 | 0.0017 | 0.6071 |
| 16 | 0.35 | 26.46 | 0.77 | 0.345 | 0.018 | 1.76 | 0.076 | 0.0378 | 0.0011 | 0.6739 |
| 17 | 0.97 | 1.24 | 0.08 | 0.864 | 0.078 | 87.9 | 6.2 | 0.806 | 0.055 | 0.967 |
| 18 | 0.69 | 14.84 | 0.64 | 0.632 | 0.042 | 5.69 | 0.32 | 0.0674 | 0.0029 | 0.7651 |
| 19 | 0.24 | 31.626 | 0.850 | 0.248 | 0.011 | 1.062 | 0.047 | 0.03162 | 0.00085 | 0.60741 |
| 20 | 0.23 | 31.260 | 0.889 | 0.241 | 0.011 | 1.051 | 0.044 | 0.03199 | 0.00091 | 0.67948 |
| 21 | 0.25 | 31.15 | 0.77 | 0.259 | 0.012 | 1.13 | 0.047 | 0.0321 | 0.0008 | 0.5917 |
| 22 | 0.37 | 24.45 | 0.84 | 0.362 | 0.019 | 2.013 | 0.1 | 0.0409 | 0.0014 | 0.6890 |
| 23 | 0.76 | 12.47 | 0.50 | 0.684 | 0.036 | 7.42 | 0.33 | 0.0802 | 0.0032 | 0.8972 |
| 24 | 0.46 | 22.78 | 0.83 | 0.436 | 0.026 | 2.58 | 0.14 | 0.0439 | 0.0016 | 0.6717 |
| 25 | 0.49 | 21.01 | 0.66 | 0.46 | 0.03 | 2.98 | 0.17 | 0.0476 | 0.0015 | 0.5524 |
| 26 | 0.33 | 27.36 | 0.82 | 0.329 | 0.017 | 1.642 | 0.085 | 0.0366 | 0.0011 | 0.5814 |
| 27 | 0.48 | 20.79 | 0.73 | 0.451 | 0.023 | 2.96 | 0.14 | 0.0481 | 0.0017 | 0.7473 |
| 28 | 0.39 | 23.92 | 0.92 | 0.373 | 0.026 | 2.1 | 0.14 | 0.0418 | 0.0016 | 0.5742 |
| 29 | 0.29 | 29.842 | 0.819 | 0.29 | 0.02 | 1.327 | 0.062 | 0.03351 | 0.00092 | 0.58761 |
| 30 | 0.86 | 7.310 | 0.310 | 0.772 | 0.043 | 14.52 | 0.72 | 0.1368 | 0.0058 | 0.8550 |
| 31 | 0.75 | 9.81 | 0.578 | 0.677 | 0.058 | 8.96 | 0.63 | 0.102 | 0.006 | 0.837 |
| 32 | 0.93 | 1.61 | 0.07 | 0.831 | 0.043 | 69.2 | 3.4 | 0.622 | 0.029 | 0.949 |

Table S5. U–Pb isotope ratios of titanite samples.

Subscript "in": initial; subscript "rad": radiogenic. First and second sessions at the University of Milan (Italy); third session at the University of Bern (Switzerland).

| Spot | f_{206} | $^{238}\text{U}/^{206}\text{U}$ | 2 S.E. | $^{207}\text{Pb}/^{206}\text{Pb}$ | 2 S.E. | $^{207}\text{Pb}/^{235}\text{U}$ | 2 S.E. | $^{206}\text{Pb}/^{238}\text{U}$ | 2 S.E. | rho | $(^{207}\text{Pb}/^{206}\text{Pb})_{\text{in}}$ | $(^{207}\text{Pb}/^{206}\text{Pb})_{\text{rad}}$ |
|----------------------------|-----------|---------------------------------|---------|-----------------------------------|---------|----------------------------------|--------|----------------------------------|---------|---------|---|--|
| Sample GT1 (first session) | | | | | | | | | | | | |
| 1 | 0.85 | 11.033 | 0.397 | 0.7187 | 0.0295 | 9.0080 | 0.3543 | 0.09064 | 0.00326 | 0.91449 | 0.841 | 0.04749 |
| 2 | 0.82 | 9.0588 | 0.7681 | 0.69855 | 0.08698 | 10.639 | 1.083 | 0.11039 | 0.00936 | 0.83279 | | |
| 3 | 0.95 | 6.298 | 0.489 | 0.80466 | 0.08522 | 17.70 | 1.51 | 0.1588 | 0.0123 | 0.9074 | | |
| 4 | 0.84 | 3.712 | 0.441 | 0.71151 | 0.12034 | 26.57 | 3.69 | 0.2694 | 0.0320 | 0.8556 | | |
| 5 | 1.00 | 4.1957 | 0.3496 | 0.84378 | 0.09308 | 27.868 | 2.498 | 0.23834 | 0.01986 | 0.92979 | | |
| 6 | 1.01 | 2.9658 | 0.3082 | 0.84696 | 0.11472 | 39.575 | 4.370 | 0.33718 | 0.03504 | 0.94111 | | |
| 7 | 0.82 | 10.896 | 0.444 | 0.69776 | 0.03508 | 8.8656 | 0.4045 | 0.09178 | 0.00374 | 0.89317 | | |
| 8 | 0.98 | 6.878 | 0.443 | 0.82906 | 0.07096 | 16.63 | 1.17 | 0.1454 | 0.0094 | 0.9148 | | |
| 9 | 0.96 | 0.84534 | 0.06394 | 0.80904 | 0.06572 | 132.63 | 10.68 | 1.18295 | 0.08948 | 0.93926 | | |
| 10 | 0.97 | 3.4344 | 0.2213 | 0.81528 | 0.06742 | 32.896 | 2.308 | 0.29117 | 0.01876 | 0.91828 | | |
| 11 | 0.90 | 3.1419 | 0.2802 | 0.75986 | 0.09094 | 33.504 | 3.344 | 0.31828 | 0.02838 | 0.89342 | | |

| | | | | | | | | | | |
|----|------|---------|---------|---------|---------|--------|--------|---------|---------|---------|
| 12 | 0.90 | 3.1682 | 0.1879 | 0.7616 | 0.0577 | 33.298 | 2.190 | 0.31564 | 0.01872 | 0.90173 |
| 13 | 0.78 | 13.20 | 0.80 | 0.66408 | 0.05814 | 6.969 | 0.511 | 0.0758 | 0.0046 | 0.8281 |
| 14 | 0.81 | 13.759 | 0.753 | 0.68759 | 0.05234 | 6.9190 | 0.4441 | 0.07268 | 0.00398 | 0.8532 |
| 15 | 0.90 | 8.826 | 0.408 | 0.7594 | 0.0447 | 11.92 | 0.61 | 0.1133 | 0.0052 | 0.9023 |
| 16 | 0.92 | 0.23062 | 0.03021 | 0.77427 | 0.07696 | 465.51 | 63.18 | 4.33619 | 0.56808 | 0.96534 |
| 17 | 0.88 | 2.319 | 0.234 | 0.74379 | 0.10066 | 44.52 | 5.15 | 0.4312 | 0.0435 | 0.8719 |
| 18 | 0.90 | 1.4841 | 0.1354 | 0.76169 | 0.08596 | 71.164 | 7.192 | 0.67381 | 0.06146 | 0.90247 |
| 19 | 0.83 | 7.0681 | 0.3727 | 0.71 | 0.05 | 13.935 | 0.840 | 0.14148 | 0.00746 | 0.87446 |
| 20 | 0.89 | 4.8109 | 0.2907 | 0.7523 | 0.0605 | 21.614 | 1.475 | 0.20786 | 0.01256 | 0.88568 |
| 21 | 0.93 | 0.7973 | 0.0814 | 0.78835 | 0.08784 | 136.7 | 14.9 | 1.254 | 0.128 | 0.9350 |
| 22 | 0.90 | 5.2673 | 0.2669 | 0.761 | 0.049 | 20.046 | 1.123 | 0.18985 | 0.00962 | 0.90487 |

Sample OSJ1002 (second session)

| | | | | | | | | | | | | |
|----|------|--------|--------|--------|--------|--------|-------|--------|--------|--------|-------|---------|
| 1 | 0.91 | 1.3164 | 0.0401 | 0.7869 | 0.0204 | 82.412 | 2.540 | 1.3164 | 0.0401 | 0.9893 | 0.861 | 0.05637 |
| 2 | 0.90 | 1.1901 | 0.0372 | 0.7829 | 0.0211 | 90.689 | 2.871 | 1.1901 | 0.0372 | 0.9866 | | |
| 3 | 0.91 | 1.4394 | 0.0467 | 0.7850 | 0.0231 | 75.190 | 2.486 | 1.4394 | 0.0467 | 0.9804 | | |
| 4 | 0.94 | 0.9849 | 0.0301 | 0.8150 | 0.0208 | 114.1 | 3.5 | 0.9849 | 0.0301 | 0.9931 | | |
| 5 | 0.98 | 0.5029 | 0.0244 | 0.8426 | 0.0365 | 230.9 | 11.6 | 0.5029 | 0.0244 | 0.9632 | | |
| 6 | 0.93 | 1.1605 | 0.0375 | 0.8012 | 0.0228 | 95.19 | 3.12 | 1.1605 | 0.0375 | 0.9853 | | |
| 7 | 0.43 | 7.7435 | 0.4629 | 0.4033 | 0.0392 | 7.181 | 0.619 | 7.7435 | 0.4629 | 0.6931 | | |
| 8 | 0.92 | 1.1885 | 0.0390 | 0.7951 | 0.0233 | 92.236 | 3.077 | 1.1885 | 0.0390 | 0.9825 | | |
| 9 | 0.54 | 5.7981 | 0.2952 | 0.4888 | 0.0361 | 11.62 | 0.76 | 5.7981 | 0.2952 | 0.7734 | | |
| 10 | 0.93 | 1.1552 | 0.0353 | 0.8009 | 0.0206 | 95.585 | 2.943 | 1.1552 | 0.0353 | 0.9920 | | |
| 11 | 0.89 | 1.5932 | 0.0480 | 0.7729 | 0.0198 | 66.884 | 2.036 | 1.5932 | 0.0480 | 0.9893 | | |
| 12 | 0.92 | 1.0319 | 0.0326 | 0.7933 | 0.0214 | 105.99 | 3.39 | 1.0319 | 0.0326 | 0.9887 | | |
| 13 | 0.70 | 4.4332 | 0.2146 | 0.6203 | 0.0390 | 19.291 | 1.084 | 4.4332 | 0.2146 | 0.8613 | | |
| 14 | 0.92 | 0.7939 | 0.0269 | 0.7940 | 0.0234 | 137.9 | 4.7 | 0.7939 | 0.0269 | 0.9840 | | |
| 15 | 0.91 | 1.0959 | 0.0345 | 0.7897 | 0.0214 | 99.343 | 3.166 | 1.0959 | 0.0345 | 0.9875 | | |
| 16 | 0.91 | 1.3754 | 0.0407 | 0.7889 | 0.0192 | 79.085 | 2.353 | 1.3754 | 0.0407 | 0.9947 | | |
| 17 | 0.90 | 1.3553 | 0.0399 | 0.7791 | 0.0187 | 79.263 | 2.342 | 1.3553 | 0.0399 | 0.9953 | | |
| 18 | 0.90 | 1.3924 | 0.0407 | 0.7787 | 0.0185 | 77.103 | 2.262 | 1.3924 | 0.0407 | 0.9956 | | |
| 19 | 0.59 | 4.5668 | 0.2311 | 0.5345 | 0.0377 | 16.137 | 1.016 | 4.5668 | 0.2311 | 0.8039 | | |
| 20 | 0.61 | 5.3505 | 0.1763 | 0.5471 | 0.0193 | 14.097 | 0.512 | 5.3505 | 0.1763 | 0.9081 | | |
| 21 | 0.93 | 1.2757 | 0.0396 | 0.8049 | 0.0214 | 86.993 | 2.738 | 1.2757 | 0.0396 | 0.9872 | | |
| 22 | 0.87 | 1.3698 | 0.0432 | 0.7532 | 0.0214 | 75.807 | 2.448 | 1.3698 | 0.0432 | 0.9774 | | |
| 23 | 0.88 | 1.4974 | 0.0491 | 0.7610 | 0.0231 | 70.072 | 2.357 | 1.4974 | 0.0491 | 0.9759 | | |
| 24 | 0.88 | 1.5204 | 0.0565 | 0.7612 | 0.0281 | 69.041 | 2.679 | 1.5204 | 0.0565 | 0.9582 | | |
| 25 | 0.87 | 1.7257 | 0.0535 | 0.7533 | 0.0207 | 60.184 | 1.900 | 1.7257 | 0.0535 | 0.9819 | | |
| 26 | 0.89 | 1.4141 | 0.0495 | 0.7736 | 0.0257 | 75.434 | 2.726 | 1.4141 | 0.0495 | 0.9680 | | |
| 27 | 0.59 | 5.5766 | 0.2028 | 0.5333 | 0.0229 | 13.186 | 0.551 | 5.5766 | 0.2028 | 0.8693 | | |
| 28 | 0.94 | 0.8502 | 0.0640 | 0.8099 | 0.0644 | 131.4 | 10.4 | 0.8502 | 0.0640 | 0.9533 | | |
| 29 | 0.89 | 1.5378 | 0.0484 | 0.7685 | 0.0215 | 68.90 | 2.20 | 1.5378 | 0.0484 | 0.9831 | | |
| 30 | 0.91 | 1.1860 | 0.0365 | 0.7870 | 0.0206 | 91.487 | 2.841 | 1.1860 | 0.0365 | 0.9900 | | |
| 31 | 0.91 | 1.1617 | 0.0346 | 0.7921 | 0.0194 | 94.025 | 2.815 | 1.1617 | 0.0346 | 0.9949 | | |
| 32 | 0.93 | 0.8922 | 0.0271 | 0.8047 | 0.0201 | 124.4 | 3.8 | 0.8922 | 0.0271 | 0.9945 | | |

| | | | | | | | | | | |
|----|------|--------|--------|--------|--------|--------|-------|--------|--------|--------|
| 33 | 0.92 | 0.9265 | 0.0295 | 0.7997 | 0.0218 | 119.0 | 3.8 | 0.9265 | 0.0295 | 0.9886 |
| 34 | 0.86 | 1.8994 | 0.0602 | 0.7497 | 0.0217 | 54.423 | 1.764 | 1.8994 | 0.0602 | 0.9772 |
| 35 | 0.87 | 1.5399 | 0.0491 | 0.7538 | 0.0218 | 67.497 | 2.200 | 1.5399 | 0.0491 | 0.9790 |
| 36 | 0.89 | 1.5966 | 0.0513 | 0.7750 | 0.0227 | 66.928 | 2.192 | 1.5966 | 0.0513 | 0.9806 |
| 37 | 0.90 | 1.5501 | 0.0491 | 0.7768 | 0.0221 | 69.101 | 2.227 | 1.5501 | 0.0491 | 0.9822 |
| 38 | 0.86 | 1.7917 | 0.0565 | 0.7498 | 0.0215 | 57.699 | 1.860 | 1.7917 | 0.0565 | 0.9784 |
| 39 | 0.82 | 1.9479 | 0.0703 | 0.7163 | 0.0265 | 50.705 | 1.931 | 1.9479 | 0.0703 | 0.9480 |
| 40 | 0.88 | 1.6384 | 0.0536 | 0.7669 | 0.0233 | 64.538 | 2.161 | 1.6384 | 0.0536 | 0.9765 |
| 41 | 0.90 | 1.4029 | 0.0439 | 0.7769 | 0.0215 | 76.352 | 2.430 | 1.4029 | 0.0439 | 0.9840 |
| 42 | 0.79 | 2.7122 | 0.0856 | 0.6956 | 0.0208 | 35.364 | 1.156 | 2.7122 | 0.0856 | 0.9654 |
| 43 | 0.88 | 1.5496 | 0.0469 | 0.7662 | 0.0200 | 68.176 | 2.089 | 1.5496 | 0.0469 | 0.9872 |
| 44 | 0.87 | 1.5351 | 0.0617 | 0.7537 | 0.0314 | 67.716 | 2.883 | 1.5351 | 0.0617 | 0.9440 |

Sample R5 (second session)

| | | | | | | | | | | | | |
|----|------|-------|-------|--------|--------|-------|-------|--------|--------|--------|-------|---------|
| 1 | 0.23 | 10.11 | 0.30 | 0.2428 | 0.0085 | 3.312 | 0.124 | 0.0989 | 0.0030 | 0.8037 | 0.861 | 0.05637 |
| 2 | 0.24 | 9.963 | 0.300 | 0.2474 | 0.0084 | 3.424 | 0.126 | 0.1004 | 0.0030 | 0.8195 | | |
| 3 | 0.08 | 12.23 | 0.34 | 0.1236 | 0.0037 | 1.394 | 0.047 | 0.0818 | 0.0023 | 0.8310 | | |
| 4 | 0.58 | 5.947 | 0.195 | 0.5200 | 0.0186 | 12.06 | 0.44 | 0.1681 | 0.0055 | 0.8954 | | |
| 5 | 0.26 | 10.27 | 0.32 | 0.2631 | 0.0097 | 3.531 | 0.136 | 0.0973 | 0.0030 | 0.7977 | | |
| 6 | 0.33 | 9.222 | 0.298 | 0.3181 | 0.0126 | 4.756 | 0.192 | 0.1084 | 0.0035 | 0.8009 | | |
| 7 | 0.13 | 11.57 | 0.33 | 0.1645 | 0.0052 | 1.959 | 0.069 | 0.0864 | 0.0025 | 0.8162 | | |
| 8 | 0.35 | 9.013 | 0.317 | 0.3390 | 0.0157 | 5.186 | 0.237 | 0.1110 | 0.0039 | 0.7703 | | |
| 9 | 0.13 | 11.56 | 0.33 | 0.1623 | 0.0048 | 1.937 | 0.066 | 0.0865 | 0.0025 | 0.8405 | | |
| 10 | 0.13 | 11.62 | 0.33 | 0.1589 | 0.0051 | 1.886 | 0.067 | 0.0861 | 0.0025 | 0.8118 | | |
| 11 | 0.32 | 8.803 | 0.282 | 0.3104 | 0.0120 | 4.862 | 0.193 | 0.1136 | 0.0036 | 0.8053 | | |
| 12 | 0.15 | 11.54 | 0.34 | 0.1808 | 0.0059 | 2.160 | 0.077 | 0.0866 | 0.0025 | 0.8143 | | |
| 13 | 0.54 | 5.824 | 0.195 | 0.4943 | 0.0187 | 11.70 | 0.45 | 0.1717 | 0.0058 | 0.8780 | | |
| 14 | 0.74 | 3.570 | 0.113 | 0.6491 | 0.0201 | 25.07 | 0.83 | 0.2801 | 0.0089 | 0.9522 | | |
| 15 | 0.13 | 11.60 | 0.34 | 0.1634 | 0.0053 | 1.942 | 0.070 | 0.0862 | 0.0025 | 0.8077 | | |
| 16 | 0.17 | 10.96 | 0.32 | 0.1901 | 0.0064 | 2.391 | 0.088 | 0.0912 | 0.0027 | 0.8019 | | |
| 17 | 0.19 | 10.93 | 0.32 | 0.2124 | 0.0071 | 2.680 | 0.097 | 0.0915 | 0.0027 | 0.8162 | | |
| 18 | 0.13 | 11.73 | 0.34 | 0.1637 | 0.0054 | 1.924 | 0.070 | 0.0852 | 0.0025 | 0.8005 | | |
| 19 | 0.25 | 9.630 | 0.304 | 0.2593 | 0.0102 | 3.713 | 0.151 | 0.1038 | 0.0033 | 0.7756 | | |
| 20 | 0.23 | 10.38 | 0.30 | 0.2403 | 0.0075 | 3.192 | 0.110 | 0.0964 | 0.0028 | 0.8489 | | |
| 21 | 0.29 | 9.419 | 0.284 | 0.2881 | 0.0095 | 4.218 | 0.150 | 0.1062 | 0.0032 | 0.8475 | | |
| 22 | 0.20 | 10.62 | 0.31 | 0.2183 | 0.0069 | 2.834 | 0.099 | 0.0942 | 0.0027 | 0.8360 | | |
| 23 | 0.23 | 10.02 | 0.30 | 0.2385 | 0.0086 | 3.282 | 0.125 | 0.0998 | 0.0030 | 0.7957 | | |
| 24 | 0.14 | 11.47 | 0.34 | 0.1675 | 0.0059 | 2.014 | 0.077 | 0.0872 | 0.0026 | 0.7673 | | |
| 25 | 0.22 | 10.40 | 0.32 | 0.2325 | 0.0085 | 3.083 | 0.119 | 0.0962 | 0.0029 | 0.7878 | | |
| 26 | 0.44 | 7.606 | 0.238 | 0.4107 | 0.0140 | 7.445 | 0.267 | 0.1315 | 0.0041 | 0.8730 | | |
| 27 | 0.12 | 11.84 | 0.35 | 0.1555 | 0.0059 | 1.812 | 0.073 | 0.0845 | 0.0025 | 0.7416 | | |
| 28 | 0.22 | 10.35 | 0.31 | 0.2349 | 0.0081 | 3.131 | 0.116 | 0.0966 | 0.0029 | 0.8082 | | |

Sample GT1 (third session)

| | | | | | | | | | | | | |
|---|------|-------|-------|------|------|-------|------|--------|--------|--------|-------|---------|
| 1 | 0.90 | 9.625 | 0.204 | 0.76 | 0.02 | 10.85 | 0.24 | 0.1039 | 0.0022 | 0.9573 | 0.841 | 0.04747 |
| 2 | 0.88 | 12.0 | 0.4 | 0.74 | 0.03 | 8.33 | 0.26 | 0.083 | 0.003 | 1.1566 | | |

| | | | | | | | | | | |
|----|------|-------|-------|-------|-------|-------|-------|--------|--------|--------|
| 3 | 0.99 | 5.807 | 0.196 | 0.831 | 0.029 | 19.49 | 0.7 | 0.1722 | 0.0058 | 0.9378 |
| 4 | 0.96 | 3.87 | 0.14 | 0.807 | 0.038 | 28.7 | 1.3 | 0.258 | 0.009 | 0.7784 |
| 5 | 0.89 | 10.09 | 0.18 | 0.754 | 0.014 | 10.29 | 0.2 | 0.0991 | 0.0018 | 0.9345 |
| 6 | 0.97 | 1.62 | 0.07 | 0.819 | 0.029 | 69.1 | 3.3 | 0.618 | 0.028 | 0.9487 |
| 7 | 0.90 | 8.897 | 0.166 | 0.764 | 0.016 | 11.79 | 0.24 | 0.1124 | 0.0021 | 0.9178 |
| 8 | 0.95 | 6.8 | 0.2 | 0.802 | 0.033 | 16 | 0.59 | 0.15 | 0.005 | 0.8855 |
| 9 | 0.94 | 5.048 | 0.097 | 0.795 | 0.015 | 21.68 | 0.42 | 0.1981 | 0.0038 | 0.9902 |
| 10 | 0.94 | 4.995 | 0.105 | 0.792 | 0.017 | 21.76 | 0.44 | 0.2002 | 0.0042 | 1.0375 |
| 11 | 0.91 | 6.680 | 0.156 | 0.766 | 0.017 | 15.68 | 0.37 | 0.1497 | 0.0035 | 0.9908 |
| 12 | 0.91 | 8.299 | 0.234 | 0.766 | 0.014 | 12.67 | 0.35 | 0.1205 | 0.0034 | 1.0214 |
| 13 | 0.90 | 9.183 | 0.219 | 0.77 | 0.02 | 11.46 | 0.32 | 0.1089 | 0.0026 | 0.8550 |
| 14 | 0.61 | 36.46 | 0.85 | 0.531 | 0.019 | 1.994 | 0.064 | 0.0274 | 0.0006 | 0.7269 |
| 15 | 0.88 | 11.5 | 0.3 | 0.748 | 0.029 | 8.88 | 0.28 | 0.087 | 0.002 | 0.8759 |
| 16 | 0.60 | 32 | 1 | 0.526 | 0.024 | 2.3 | 0.1 | 0.03 | 0.001 | 0.7036 |
| 17 | 0.87 | 10.25 | 0.33 | 0.738 | 0.026 | 9.86 | 0.32 | 0.0976 | 0.0031 | 0.9787 |
| 18 | 0.95 | 5.1 | 0.3 | 0.805 | 0.036 | 21 | 1 | 0.20 | 0.01 | 0.9829 |
| 19 | 0.97 | 2.5 | 0.2 | 0.819 | 0.051 | 43 | 3 | 0.41 | 0.03 | 1.0345 |
| 20 | 0.94 | 5.39 | 0.23 | 0.796 | 0.037 | 20.4 | 1.0 | 0.186 | 0.008 | 0.8899 |
| 21 | 0.94 | 3.26 | 0.17 | 0.793 | 0.047 | 32.8 | 1.7 | 0.307 | 0.016 | 1.0056 |
| 22 | 1.00 | 1.55 | 0.08 | 0.84 | 0.04 | 74.4 | 3.9 | 0.647 | 0.032 | 0.9435 |
| 23 | 0.96 | 0.365 | 0.021 | 0.813 | 0.041 | 303 | 19 | 2.74 | 0.16 | 0.9312 |
| 24 | 1.03 | 6.6 | 0.4 | 0.865 | 0.086 | 17 | 1 | 0.15 | 0.01 | 0.8083 |
| 25 | 0.97 | 1.01 | 0.04 | 0.815 | 0.031 | 111 | 5 | 0.986 | 0.041 | 0.9034 |
| 26 | 0.98 | 3.26 | 0.17 | 0.829 | 0.036 | 34.3 | 1.8 | 0.307 | 0.016 | 0.9931 |
| 27 | 0.86 | 11 | 1 | 0.731 | 0.029 | 9.3 | 0.6 | 0.09 | 0.01 | 0.8660 |

A3. Zircon U–Pb geochronology

Table S6. U–Pb isotope data of OSJ-T05 zircon from Osayama.

| Spot | Pb207/ Pb206 | S.E. | Pb206/ U238 | S.E. | Pb207/ U235 | S.E. | Pb207/ U235 | S.E. | Pb206/ U238 | S.E. | Concordance | Terra-Wasserburg Concordia Plot | | | |
|------|-----------------|-------|----------------|-------|----------------|-------|----------------|--------|----------------|--------|-------------|---------------------------------|--------|-----------------|--------|
| | | | | | | | | | | | | U238/ 206Pb | 2 S.E. | 207Pb/ 206Pb | 2 S.E. |
| 1 | 0.057 | 0.003 | 0.085 | 0.002 | 0.669 | 0.036 | 520.109 | 43.768 | 523.013 | 19.495 | 1.006 | 11.832 | 0.230 | 0.057 | 0.003 |
| 2 | 0.056 | 0.002 | 0.084 | 0.001 | 0.650 | 0.024 | 508.277 | 28.944 | 519.281 | 17.297 | 1.022 | 11.921 | 0.207 | 0.056 | 0.002 |
| 3 | 0.059 | 0.001 | 0.085 | 0.001 | 0.691 | 0.018 | 533.621 | 21.105 | 525.399 | 16.541 | 0.985 | 11.776 | 0.193 | 0.059 | 0.001 |
| 4 | 0.060 | 0.002 | 0.084 | 0.002 | 0.696 | 0.028 | 536.503 | 33.592 | 521.034 | 17.898 | 0.971 | 11.879 | 0.212 | 0.060 | 0.002 |
| 5 | 0.064 | 0.002 | 0.085 | 0.002 | 0.755 | 0.028 | 570.990 | 31.884 | 528.337 | 17.840 | 0.925 | 11.708 | 0.206 | 0.064 | 0.002 |
| 6 | 0.056 | 0.002 | 0.084 | 0.001 | 0.647 | 0.021 | 506.897 | 25.603 | 519.846 | 16.934 | 1.026 | 11.907 | 0.202 | 0.056 | 0.002 |
| 7 | 0.055 | 0.003 | 0.086 | 0.002 | 0.654 | 0.034 | 510.915 | 41.347 | 530.653 | 19.370 | 1.039 | 11.655 | 0.222 | 0.055 | 0.003 |
| 8 | 0.061 | 0.002 | 0.085 | 0.002 | 0.707 | 0.030 | 543.218 | 35.847 | 523.775 | 18.319 | 0.964 | 11.814 | 0.215 | 0.061 | 0.002 |
| 9 | 0.064 | 0.003 | 0.085 | 0.002 | 0.742 | 0.041 | 563.629 | 48.237 | 523.626 | 20.007 | 0.929 | 11.818 | 0.235 | 0.064 | 0.003 |
| 10 | 0.059 | 0.001 | 0.085 | 0.001 | 0.690 | 0.020 | 533.054 | 24.239 | 524.255 | 16.850 | 0.983 | 11.803 | 0.197 | 0.059 | 0.001 |
| 11 | 0.059 | 0.002 | 0.082 | 0.002 | 0.669 | 0.030 | 520.181 | 36.463 | 510.808 | 18.042 | 0.982 | 12.127 | 0.223 | 0.059 | 0.002 |
| 12 | 0.059 | 0.003 | 0.082 | 0.002 | 0.666 | 0.033 | 518.097 | 40.703 | 509.990 | 18.652 | 0.984 | 12.147 | 0.231 | 0.059 | 0.003 |
| 13 | 0.058 | 0.001 | 0.085 | 0.001 | 0.681 | 0.019 | 527.363 | 22.459 | 525.715 | 17.226 | 0.997 | 11.769 | 0.201 | 0.058 | 0.001 |
| 14 | 0.057 | 0.002 | 0.085 | 0.002 | 0.664 | 0.028 | 517.061 | 34.146 | 523.674 | 18.588 | 1.013 | 11.817 | 0.218 | 0.057 | 0.002 |
| 15 | 0.059 | 0.002 | 0.084 | 0.002 | 0.689 | 0.031 | 532.296 | 36.723 | 522.610 | 18.902 | 0.982 | 11.842 | 0.223 | 0.059 | 0.002 |
| 16 | 0.057 | 0.002 | 0.085 | 0.001 | 0.673 | 0.021 | 522.573 | 26.090 | 526.189 | 17.655 | 1.007 | 11.758 | 0.205 | 0.057 | 0.002 |
| 17 | 0.056 | 0.002 | 0.086 | 0.002 | 0.670 | 0.029 | 520.795 | 35.645 | 532.790 | 19.077 | 1.023 | 11.606 | 0.216 | 0.056 | 0.002 |
| 18 | 0.059 | 0.002 | 0.085 | 0.002 | 0.696 | 0.023 | 536.428 | 27.764 | 526.333 | 17.828 | 0.981 | 11.755 | 0.207 | 0.059 | 0.002 |
| 19 | 0.058 | 0.001 | 0.084 | 0.001 | 0.677 | 0.021 | 525.139 | 24.971 | 521.989 | 17.388 | 0.994 | 11.856 | 0.206 | 0.058 | 0.001 |
| 20 | 0.061 | 0.003 | 0.083 | 0.002 | 0.699 | 0.038 | 538.276 | 45.563 | 516.355 | 20.027 | 0.959 | 11.991 | 0.242 | 0.061 | 0.003 |
| 21 | 0.057 | 0.003 | 0.085 | 0.002 | 0.670 | 0.033 | 520.512 | 40.071 | 524.845 | 19.459 | 1.008 | 11.789 | 0.228 | 0.057 | 0.003 |
| 22 | 0.057 | 0.001 | 0.085 | 0.001 | 0.665 | 0.020 | 517.371 | 24.181 | 527.612 | 17.482 | 1.020 | 11.725 | 0.202 | 0.057 | 0.001 |
| 23 | 0.060 | 0.002 | 0.085 | 0.002 | 0.697 | 0.027 | 536.726 | 31.882 | 523.940 | 18.271 | 0.976 | 11.810 | 0.214 | 0.060 | 0.002 |
| 24 | 0.058 | 0.001 | 0.086 | 0.001 | 0.687 | 0.019 | 530.696 | 22.654 | 529.066 | 17.338 | 0.997 | 11.691 | 0.200 | 0.058 | 0.001 |
| 25 | 0.061 | 0.002 | 0.084 | 0.002 | 0.710 | 0.029 | 544.549 | 34.660 | 521.166 | 18.528 | 0.957 | 11.876 | 0.220 | 0.061 | 0.002 |
| 26 | 0.056 | 0.003 | 0.085 | 0.002 | 0.654 | 0.037 | 510.712 | 44.962 | 524.325 | 20.162 | 1.027 | 11.801 | 0.236 | 0.056 | 0.003 |

Supplement B: Values of $\text{CH}_4/(\text{CH}_4+\text{CO}_2)$ and XC at varying FMQ and P–T conditions.

Table S7. Values of $\text{CH}_4/(\text{CH}_4 + \text{CO}_2)$ at varying FMQ and P–T conditions.

Calculated using the Thermotopes-COH software (Boutier et al., 2024). Age, location, T and P data are from Brown and Johnson (2019).

| Age [Ga] | Location | T [°C] | P [GPa] | $\text{CH}_4/(\text{CH}_4+\text{CO}_2)$ FMQ+1 | $\text{CH}_4/(\text{CH}_4+\text{CO}_2)$ FMQ | $\text{CH}_4/(\text{CH}_4+\text{CO}_2)$ FMQ-1 | $\text{CH}_4/(\text{CH}_4+\text{CO}_2)$ FMQ-2 | $\text{CH}_4/(\text{CH}_4+\text{CO}_2)$ FMQ-3 |
|----------|---|--------|---------|---|---|---|---|---|
| 1.29 | Fraser Range Metamorphics, Frazer zone, Albany-Fraser orogen, Australia | 850 | 0.9 | 0 | 0 | 0.0115 | 0.75 | 0.99 |
| 1.21 | Mutherbakin zone, Capricorn orogen, Western Australia | 650 | 0.7 | 0 | 0 | 0.219 | 0.956 | 0.998 |
| 1.2 | Kakamas terrane, central Namaqua metamorphic complex, South Africa | 900 | 0.5 | 0 | 0 | 0 | 0.485 | 0.973 |
| 1.2 | Aggeneys terrane, western Namaqua metamorphic complex, South Africa | 650 | 0.5 | 0 | 0 | 0.171 | 0.942 | 0.998 |
| 1.2 | Western Musgrave Province, Western Australia | 1000 | 0.75 | 0 | 0 | 0 | 0.326 | 0.96 |
| 1.19 | Eastern Musgrave Province, South Australia | 900 | 0.63 | 0 | 0 | 0 | 0.561 | 0.979 |
| 1.156 | Adirondack Highlands, Grenville Province, North America (average 11 samples) | 820 | 0.92 | 0 | 0 | 0.0219 | 0.802 | 0.993 |
| 1.135 | Jordan Ranch, Llano uplift, Texas | 790 | 2.4 | 0 | 0 | 0.043 | 0.834 | 0.996 |
| 1.132 | Chewings Range, Warumpi Province, central Australia | 570 | 0.35 | 0 | 0.000346 | 0.446 | 0.904 | 0.999 |
| 1.13 | Haasts Bluff domain, Warumpi Province, central Australia | 810 | 0.55 | 0 | 0 | 0.00627 | 0.738 | 0.989 |
| 1.09 | Western Central Gneiss Belt, Grenville Province, Ontario, Canada | 725 | 1.6 | 0 | 7.09×10^{-6} | 0.107 | 0.92 | 0.998 |
| 1.061 | Location 244, Canyon Domain, Manicouagan Imbricate zone, Grenville Province, Quebec, Canada | 880 | 1.5 | 0 | 0 | 0.0156 | 0.746 | 0.992 |
| 1.05 | Aus terrane, southwestern Namaqua metamorphic complex, southern Namibia | 825 | 0.55 | 0 | 0 | 0.00322 | 0.706 | 0.987 |
| 1.05 | Eastern Lelukuau terrane, Manicouagan Imbricate zone, Grenville Province, Quebec, Canada | 850 | 1.6 | 0 | 0 | 0.0256 | 0.792 | 0.994 |
| 1.046 | Southern Baie du Nord segment, Manicouagan Imbricate zone, Grenville Province, Quebec, Canada | 865 | 1.5 | 0 | 0 | 0.0199 | 0.77 | 0.993 |
| 1.046 | Lunden dike, Idefjorden terrane, Sveconorwegian orogen, southwest Sweden | 740 | 1.5 | 0 | 0 | 0.0925 | 0.91 | 0.997 |
| 1.042 | Lac Espadon suite, Manicouagan Imbricate zone, Grenville Province, Quebec, Canada | 855 | 1.7 | 0 | 0 | 0.0244 | 0.784 | 0.994 |
| 1.04 | Mollendo-Camana Block, Arequipa-Antofalla Basement, central Andean Margin | 950 | 1.15 | 0 | 0 | 0.000684 | 0.579 | 0.983 |
| 1.04 | Northern domain, Sausar mobile belt, central Indian tectonic zone | 850 | 1 | 0 | 0 | 0.0147 | 0.764 | 0.991 |
| 1.03 | Namaqualand terrane, southwestern Namaqua metamorphic complex, Namibia | 890 | 0.55 | 0 | 0 | 0 | 0.546 | 0.978 |
| 1.03 | Bamble terrane, Sveconorwegian belt, south Norway | 940 | 1.05 | 0 | 0 | 0.000577 | 0.587 | 0.983 |
| 1.03 | Chipata Terrane, southern Irumide Belt, Zambia | 1000 | 0.65 | 0 | 0 | 0 | 0.278 | 0.953 |
| 1.022 | Wakole Terrane, Ubendian Belt, Tanzania | 747 | 0.91 | 0 | 0 | 0.0713 | 0.891 | 0.996 |
| 1.015 | Garzon Massif, Colombia | 965 | 0.7 | 0 | 0 | 0 | 0.409 | 0.968 |
| 1.01 | Eclogite/websterite, eastern unit, Glenelg-Attadale inlier, northwest Scotland | 750 | 2 | 0 | 2.51×10^{-6} | 0.074 | 0.892 | 0.997 |
| 1.008 | Rogaland, Norway | 975 | 0.75 | 0 | 0 | 0 | 0.402 | 0.968 |
| 1 | Anantagiri, Eastern Ghats Province | 1020 | 0.7 | 0 | 0 | 0 | 0.243 | 0.948 |

| | | | | | | | | |
|-------|--|------|------|--------|-----------------------|----------|-------|-------|
| 1 | Sunkarametta, Eastern Ghats Province, India | 955 | 0.78 | 0 | 0 | 0 | 0.473 | 0.974 |
| 1 | Paderu, Eastern Ghats Province, India | 950 | 0.83 | 0 | 0 | 0 | 0.505 | 0.976 |
| 1 | Sostrene Island, Larsemann Hills, Prydz Bay, E Antarctica | 900 | 1 | 0 | 0 | 0.00374 | 0.67 | 0.987 |
| 0.988 | Basal shear zone, eclogite-bearing nappe, Eastern segment, Sveconorwegian orogen, southwest Sweden | 870 | 1.75 | 0 | 0 | 0.0202 | 0.762 | 0.993 |
| 0.974 | Eclogite-bearing nappe, eastern segment, Sveconorwegian orogen, southwest Sweden | 765 | 1.6 | 0 | 0 | 0.0699 | 0.888 | 0.997 |
| 0.97 | Chotanagpur gneiss complex, eastern Indian tectonic zone | 800 | 1.1 | 0 | 0 | 0.0398 | 0.844 | 0.995 |
| 0.965 | Stillwell Hills, East Antarctica | 920 | 0.87 | 0 | 0 | 0.000302 | 0.596 | 0.982 |
| 0.961 | Forbes Glacier, MacRobertson Land, East Antarctica | 910 | 0.6 | 0 | 0 | 0 | 0.519 | 0.976 |
| 0.95 | Vestfold Hills, Prydz Bay, East Antarctica | 830 | 0.9 | 0 | 0 | 0.0179 | 0.784 | 0.992 |
| 0.945 | Mawson Escarpment, Southern Prince Charles Mountains, East Antarctica | 800 | 0.68 | 0 | 0 | 0.018 | 0.794 | 0.992 |
| 0.941 | Cape Bruce, MacRobertson Land, East Antarctica | 830 | 0.6 | 0 | 0 | 0.00442 | 0.715 | 0.988 |
| 0.93 | Northern Prince Charles Mountains, East Antarctica | 865 | 0.65 | 0 | 0 | 0.00113 | 0.657 | 0.985 |
| 0.926 | Oygarden group, Kemp Land, East Antarctica | 950 | 0.85 | 0 | 0 | 0 | 0.512 | 0.977 |
| 0.825 | Korla, northern Tarim Craton, China | 685 | 1.2 | 0 | 6.94×10^{-5} | 0.171 | 0.947 | 0.998 |
| 0.82 | Welayati Formation, Kabul Block, Afghanistan | 640 | 0.9 | 0 | 0.000442 | 0.273 | 0.966 | 0.999 |
| 0.788 | NE margin Tarim craton, Tibet | 810 | 1 | 0 | 0 | 0.0307 | 0.824 | 0.994 |
| 0.788 | Polnish, Morar Group, Moine Supergroup, NW Scotland | 650 | 0.8 | 0 | 4.55×10^{-5} | 0.233 | 0.959 | 0.998 |
| 0.75 | Barro Alto complex, Northern Brasília Belt, Brazil | 980 | 0.8 | 0 | 0 | 0 | 0.407 | 0.968 |
| 0.75 | Aksu blueschist terrane, western China | 350 | 1.15 | 0.0759 | 0.892 | 0.999 | 1 | 1 |
| 0.725 | Glen Urquhart, Glenfinnan Group, Moine Supergroup, Scotland | 700 | 0.9 | 0 | 0 | 0.132 | 0.931 | 0.998 |
| 0.702 | Eidet, Kalak Nappe Complex, northern Norway | 768 | 0.93 | 0 | 0 | 0.0539 | 0.871 | 0.995 |
| 0.685 | Tighsi, Egere terrane, Central Hoggar, Algeria | 860 | 1.9 | 0 | 0 | 0.0233 | 0.773 | 0.994 |
| 0.685 | Azrou N'Fad, Central Hoggar, Algeria | 760 | 1.5 | 0 | 0 | 0.0743 | 0.893 | 0.997 |
| 0.685 | Tin Begane, Central Hoggar, Algeria | 790 | 1.5 | 0 | 0 | 0.0529 | 0.864 | 0.996 |
| 0.685 | Tighsi, Egere terrane, Central Hoggar, Algeria | 694 | 1.96 | 0 | 0.000349 | 0.131 | 0.935 | 0.999 |
| 0.685 | Adrar Izzilatène, Egere terrane, Central Hoggar, Algeria | 670 | 2 | 0 | 0.000756 | 0.164 | 0.948 | 0.999 |
| 0.655 | Central Zambia | 755 | 2.83 | 0 | 4.51×10^{-5} | 0.0471 | 0.84 | 0.997 |
| 0.653 | Xiongqian, North Lhasa, Tibet | 710 | 1.75 | 0 | 0.000118 | 0.12 | 0.929 | 0.998 |
| 0.65 | Três Pontas-Varginha Nappe, southern Brasília Belt, Brazil | 900 | 1.5 | 0 | 0 | 0.011 | 0.712 | 0.99 |
| 0.65 | Furua complex, Mahenge Mountains, southern Tanzania (average 16 samples) | 900 | 1.26 | 0 | 0 | 0.00798 | 0.7 | 0.989 |
| 0.65 | Meta-anorthosite, Uluguru Mountains, Tanzania | 900 | 1.25 | 0 | 0 | 0.00783 | 0.699 | 0.989 |
| 0.65 | Três Pontas-Varginha Nappe, southern Brasília Belt, Brazil | 900 | 3 | 0 | 0 | 0.0118 | 0.638 | 0.991 |
| 0.644 | Schirmacher Hills, East Antarctica | 800 | 0.8 | 0 | 0 | 0.0258 | 0.816 | 0.993 |
| 0.64 | Anápolis-Itaçu complex, Southern Brasília Belt, Brazil | 1000 | 0.9 | 0 | 0 | 0 | 0.382 | 0.967 |
| 0.64 | Gadel Group, Tarkhait, central Mauritaniides, West Africa | 600 | 1.1 | 0 | 0.00377 | 0.424 | 0.982 | 0.999 |

| | | | | | | | | |
|-------|---|------|------|---------|-----------------------|---------|-------|-------|
| 0.627 | Brattnipene, southwestern terrane, Sør Rondane Mountains, East Antarctica | 860 | 0.85 | 0 | 0 | 0.00736 | 0.723 | 0.989 |
| 0.623 | Tidérijaouine, Tassendjanet terrane, Western Hoggar, Algeria | 660 | 2.1 | 0 | 0.000979 | 0.174 | 0.952 | 0.999 |
| 0.621 | Guaxupé Nappe, southern Brasília Belt, Brazil | 860 | 1.1 | 0 | 0 | 0.0145 | 0.758 | 0.991 |
| 0.621 | Eclogite, southern Dahomeyide Belt, Ghana | 600 | 1.6 | 0 | 0.00424 | 0.389 | 0.982 | 1 |
| 0.62 | Eclogite, Richarddalen Complex, Biscayarhalvøya, Spitsbergen | 720 | 2 | 0 | 0.000111 | 0.0994 | 0.916 | 0.998 |
| 0.618 | Carvalhos Klippe, southern Brasília Belt, Brazil | 850 | 1.2 | 0 | 0 | 0.02 | 0.781 | 0.992 |
| 0.615 | Forquilha eclogite zone, NW Borborema Province, NE Brazil | 770 | 2.8 | 0 | 1.40×10 ⁻⁵ | 0.0421 | 0.827 | 0.997 |
| 0.613 | Cariré granulite region, NW Borborema Province, NE Brazil | 750 | 1.02 | 0 | 0 | 0.0745 | 0.894 | 0.996 |
| 0.612 | Vohibory block, southern Madagascar | 850 | 1.1 | 0 | 0 | 0.0176 | 0.774 | 0.992 |
| 0.611 | Eclogite, Gourma Nappe complex, northern Mali | 720 | 3.2 | 0 | 0.000175 | 0.0505 | 0.847 | 0.997 |
| 0.61 | Central Zambia | 755 | 2.83 | 0 | 4.51×10 ⁻⁵ | 0.0471 | 0.84 | 0.997 |
| 0.608 | Eclogite, Lato Hills, south Togo | 710 | 2.9 | 0 | 0.000244 | 0.0673 | 0.88 | 0.998 |
| 0.605 | NE Ox Inlier, NW Ireland | 875 | 1.45 | 0 | 0 | 0.0164 | 0.753 | 0.992 |
| 0.604 | Central African fold belt, north-central Cameroon | 875 | 1.2 | 0 | 0 | 0.0125 | 0.741 | 0.991 |
| 0.602 | Sabaloka, eastern margin of the east Sahara ghost craton, north Sudan | 950 | 0.55 | 0 | 0 | 0 | 0.37 | 0.963 |
| 0.593 | Eclogite, Ubendian Belt, Tanzania | 740 | 1.8 | 0 | 2.19×10 ⁻⁶ | 0.0873 | 0.905 | 0.998 |
| 0.589 | Turvo-Cajati Formation, Curitiba terrane, Ribeira Belt, Brazil | 790 | 1.13 | 0 | 0 | 0.0468 | 0.857 | 0.957 |
| 0.586 | Mather Peninsula, Rauer Islands, Prydz Bay, E Antarctica | 1010 | 1.1 | 0 | 0 | 0 | 0.405 | 0.97 |
| 0.58 | Southern Victoria Land, Ross orogen, Antarctica | 675 | 0.55 | 0 | 0 | 0.127 | 0.927 | 0.997 |
| 0.577 | Rio de Janeiro city outcrops, Costeiro domain, Oriental terrane, Ribeira Belt, Brazil | 800 | 0.7 | 0 | 0 | 0.0194 | 0.798 | 0.992 |
| 0.57 | Central Highland Complex, Sri Lanka | 950 | 0.9 | 0 | 0 | 0 | 0.526 | 0.978 |
| 0.57 | Brattskarvet, Eastern H.U. Sverdrupfjella, East Antarctica | 930 | 1.45 | 0 | 0 | 0.00526 | 0.653 | 0.987 |
| 0.57 | Shear zones, Bates region, Musgrave Block, Australia | 750 | 1.2 | 0 | 0 | 0.0807 | 0.9 | 0.997 |
| 0.56 | Kanjampara, central Trivandrum block (Kerala Khondalite Belt), India | 850 | 0.65 | 0 | 0 | 0.00287 | 0.691 | 0.987 |
| 0.56 | Nagercoil block, southern India | 930 | 0.7 | 0 | 0 | 0 | 0.511 | 0.976 |
| 0.56 | Western Mann Ranges, Musgrave Block, Australia | 735 | 1.2 | 0 | 0 | 0.0965 | 0.913 | 0.997 |
| 0.555 | Rundvågshetta, Lutzow-Holm Bay, East Antarctica | 1000 | 1 | 0 | 0 | 0 | 0.411 | 0.97 |
| 0.553 | Blueschist, Anglesey, UK | 415 | 0.8 | 0.00589 | 0.424 | 0.985 | 1 | 1 |
| 0.552 | Kakkod, central Trivandrum block (Kerala Khondalite Belt), India | 875 | 0.8 | 0 | 0 | 0.00327 | 0.681 | 0.987 |
| 0.55 | Southern Granulite Terrain, India | 1000 | 1.25 | 0 | 0 | 0 | 0.462 | 0.975 |
| 0.55 | Davenport shear zone, Musgrave Ranges, Musgrave Block, Australia | 650 | 1.2 | 0 | 0.000761 | 0.252 | 0.965 | 0.999 |
| 0.545 | McKaskle Hills, East Amery Ice Shelf, East Antarctica | 865 | 0.7 | 0 | 0 | 0.00222 | 0.675 | 0.986 |
| 0.545 | Grove Mountains, East Antarctica | 805 | 1.3 | 0 | 0 | 0.042 | 0.846 | 0.995 |
| 0.545 | Kuiseb River, Damara Belt, Namibia | 610 | 1.07 | 0 | 0.00269 | 0.384 | 0.979 | 0.999 |
| 0.544 | Achankovil zone, southern India | 950 | 0.7 | 0 | 0 | 0 | 0.454 | 0.987 |
| 0.54 | Bemarivo Belt, northern Madagascar | 950 | 0.9 | 0 | 0 | 0 | 0.526 | 0.978 |

| | | | | | | | | |
|-------|--|------|-------|------------------------|-----------------------|---------|-------|-------|
| 0.54 | Anosyen domain, southeastern Madagascar | 900 | 0.625 | 0 | 0 | 0 | 0.559 | 0.968 |
| 0.537 | Kumdy-Kol, Kokchetav Massif, northern Kazakhstan | 1035 | 7 | 0 | 0 | 0.00142 | 0.159 | 0.948 |
| 0.53 | Whiteschits, Solwezi dome, internal zone Lufilian Arc, Zambia | 750 | 1.3 | 0 | 0 | 0.0824 | 0.901 | 0.997 |
| 0.529 | Gjelsvikfjella, Central Maud belt, East Antarctica | 747 | 0.825 | 0 | 0 | 0.065 | 0.885 | 0.996 |
| 0.528 | Barchi-Kol, Kokchetav Massif, northern Kazakhstan | 1000 | 4.9 | 0 | 0 | 0.00251 | 0.301 | 0.974 |
| 0.525 | Panagad, Palghat Cauvery shear system, Southern Indian | 930 | 0.76 | 0 | 0 | 0 | 0.535 | 0.978 |
| 0.525 | Kaoko Belt, Namibia | 750 | 0.8 | 0 | 0 | 0.0602 | 0.88 | 0.995 |
| 0.525 | Búzios succession, Cabo Frio tectonic domain, Brazil | 760 | 0.9 | 0 | 0 | 0.0587 | 0.877 | 0.996 |
| 0.525 | Ultramafic rocks, Shackleton Range, East Antarctica | 825 | 2.3 | 0 | 0 | 0.0319 | 0.8 | 0.995 |
| 0.524 | Mawson Escarpement, Southern Prince Charles Mountains, East Antarctica | 630 | 0.6 | 0 | 9.83×10^{-7} | 0.26 | 0.962 | 0.998 |
| 0.52 | Central Damara Belt, Namibia | 750 | 0.5 | 0 | 0 | 0.0266 | 0.828 | 0.993 |
| 0.515 | Taylor/Brocklehurst/Meredith, Northern Prince Charles Mountains, East Antarctica | 810 | 0.63 | 0 | 0 | 0.0111 | 0.764 | 0.99 |
| 0.511 | Collingwood River, Franklin Metamorphic Complex, Tasmania | 630 | 1.8 | 0 | 0.00207 | 0.0269 | 0.97 | 0.999 |
| 0.51 | Madras Granulites, India (average 8 samples) | 860 | 0.85 | 0 | 0 | 0.00736 | 0.723 | 0.989 |
| 0.5 | South-west Altyn Tagh, China | 830 | 2.9 | 0 | 0 | 0.0238 | 0.746 | 0.995 |
| 0.5 | Lanternman Range, Northern Victoria Land, Antarctica | 800 | 3.2 | 0 | 2.81×10^{-7} | 0.261 | 0.753 | 0.995 |
| 0.495 | South Altyn Tagh, NW China | 950 | 2.14 | 0 | 0 | 0.00628 | 0.614 | 0.988 |
| 0.494 | Eclogite, North Qinling, China | 700 | 2.75 | 0 | 0.000325 | 0.0812 | 0.899 | 0.998 |
| 0.491 | Eclogite, Attunga, southern New England Orogen, Australia | 650 | 2.24 | 0 | 0.0012 | 0.179 | 0.954 | 0.999 |
| 0.49 | Port Macquarie, New South Wales, Australia | 590 | 2.7 | 8.22×10^{-10} | 0.00296 | 0.263 | 0.972 | 1 |
| 0.49 | Dia eclogite, North Qinling, China | 689 | 3.5 | 0 | 0.000302 | 0.054 | 0.926 | 0.998 |
| 0.477 | Migmatite, Sierra de Valle Fértil, Famatinian magmatic arc, Argentina | 825 | 0.66 | 0 | 0 | 0.00834 | 0.745 | 0.989 |
| 0.474 | Lunna Ness, Mainland, Shetland | 775 | 1 | 0 | 0 | 0.0522 | 0.867 | 0.995 |
| 0.474 | Aktyuz, Northern Tianshan, Kyrgyzstan | 600 | 2.3 | 0 | 0.0032 | 0.294 | 0.975 | 1 |
| 0.471 | Jaeren nappe, SW Norway | 620 | 2.55 | 0 | 0.00189 | 0.207 | 0.961 | 0.999 |
| 0.47 | Carpholite blueschists, Motalafjella, Spitsbergen | 400 | 1.55 | 0.00776 | 0.452 | 0.988 | 1 | 1 |
| 0.47 | Blueschist, Nordenskiöld Land, Spitsbergen | 480 | 1.6 | 0.000423 | 0.0647 | 0.875 | 0.998 | 1 |
| 0.47 | Makbal, Northern Tianshan, Kyrgyzstan | 555 | 3.05 | 1.17×10^{-5} | 0.00427 | 0.318 | 0.978 | 1 |
| 0.467 | Naver Nappe, Moine Supergroup, north Sutherland, Scotland | 675 | 1.15 | 0 | 0.000135 | 0.191 | 0.952 | 0.998 |
| 0.466 | North Qilian, China | 540 | 2.2 | 2.71×10^{-5} | 0.0112 | 0.552 | 0.991 | 1 |
| 0.465 | Eclogite, Chinese Beishan, southern Altai | 760 | 1.6 | 0 | 0 | 0.0738 | 0.892 | 0.997 |
| 0.462 | Harts Range meta-igneous complex, central Australia | 880 | 1.05 | 0 | 0 | 0.00825 | 0.717 | 0.989 |
| 0.46 | Eclogite, Bakersville, Eastern Blue Ridge, Southern Appalachians | 700 | 1.6 | 0 | 0.00015 | 0.139 | 0.937 | 0.998 |
| 0.46 | Stor Jougdan, Seve Nappe Complex, Sweden | 815 | 3.5 | 0 | 0 | 0.0195 | 0.698 | 0.994 |
| 0.456 | Northwest Connecticut, USA | 710 | 1.45 | 0 | 2.35×10^{-5} | 0.129 | 0.932 | 0.998 |
| 0.452 | Tromsø Nappe, Norway | 770 | 3.5 | 0 | 3.22×10^{-5} | 0.0275 | 0.755 | 0.996 |
| 0.446 | Tjeliken eclogite, Seve nappe complex, Sweden | 660 | 2.5 | 0 | 0.00088 | 0.14 | 0.94 | 0.999 |
| 0.445 | Dulan, North Qaidam, NW China | 892 | 3.68 | 0 | 0 | 0.00969 | 0.571 | 0.99 |

| | | | | | | | | |
|-------|---|------|------|-----------------------|-----------------------|----------|-------|-------|
| 0.442 | Ky-Grt gneiss, Areskutan, Seve nappe complex, Sweden | 650 | 2.8 | 0 | 0.000931 | 0.129 | 0.935 | 0.999 |
| 0.44 | Lower unit, Kuanping Group, Tongbai Orogen | 590 | 1.03 | 0 | 0.00475 | 0.466 | 0.984 | 0.999 |
| 0.44 | Eidet, Kalak Nappe Complex, northern Norway | 630 | 1.13 | 0 | 0.00148 | 0.312 | 0.973 | 0.999 |
| 0.435 | Dulan, North Qaidam, western China | 870 | 1.7 | 0 | 0 | 0.0199 | 0.763 | 0.993 |
| 0.435 | Dulan, North Qaidam, western China | 850 | 1.7 | 0 | 0 | 0.0261 | 0.791 | 0.994 |
| 0.435 | Xitieshan, North Qaidam, NW China | 770 | 2.95 | 0 | 1.93×10^{-5} | 0.0386 | 0.814 | 0.996 |
| 0.433 | Yuka, North Qaidam, NW China | 652 | 3.01 | 0 | 0.000794 | 0.11 | 0.924 | 0.999 |
| 0.432 | Metabasic rock, Roan, Vestranden, northern Western Gneiss region, Norway | 870 | 1.45 | 0 | 0 | 0.0178 | 0.761 | 0.992 |
| 0.431 | Dunhuang, Tarin Craton | 780 | 1.5 | 0 | 0 | 0.0594 | 0.874 | 0.996 |
| 0.43 | Wilmington complex, Delaware, USA | 800 | 0.7 | 0 | 0 | 0.0194 | 0.798 | 0.992 |
| 0.43 | Holsnøy, Bergen Arca, Norway | 750 | 1.8 | 0 | 0 | 0.0788 | 0.897 | 0.997 |
| 0.428 | East Kunlun, western China | 620 | 1.6 | 0 | 0.00265 | 0.319 | 0.976 | 0.999 |
| 0.426 | Qinling Group, Tongbai Orogen, China | 800 | 0.85 | 0 | 0 | 0.0287 | 0.823 | 0.993 |
| 0.425 | Xiangtaohu, central Qiantang, Tibet | 845 | 1.3 | 0 | 0 | 0.0238 | 0.794 | 0.993 |
| 0.425 | Jættedal complex, Liverpool Land, East Greenland | 850 | 1.1 | 0 | 0 | 0.0176 | 0.774 | 0.992 |
| 0.412 | Limousin, Massif Central, France | 660 | 3 | 0 | 0.000689 | 0.102 | 0.918 | 0.999 |
| 0.41 | Northern UHP domain, Western Gneiss Region, Norway | 815 | 3.25 | 0 | 0 | 0.0225 | 0.728 | 0.995 |
| 0.41 | Southern and Central UHP domains, Western Gneiss Region, Norway | 800 | 3.5 | 0 | 2.85×10^{-6} | 0.0219 | 0.717 | 0.995 |
| 0.408 | Monts du Lyonnais, Massif Central, France | 750 | 2.8 | 0 | 5.75×10^{-5} | 0.0501 | 0.848 | 0.997 |
| 0.403 | Eclogite, Punta de li Tulchi, Sardinia | 690 | 1.9 | 0 | 0.000388 | 0.14 | 0.939 | 0.999 |
| 0.401 | Góry Sowie Mountains, southwest Poland | 900 | 1.5 | 0 | 0 | 0.011 | 0.712 | 0.99 |
| 0.4 | Payer Land, NE Greenland | 825 | 1.6 | 0 | 0 | 0.0352 | 0.824 | 0.995 |
| 0.399 | Lofoten, Norway | 665 | 2.65 | 0 | 0.000745 | 0.122 | 0.931 | 0.999 |
| 0.399 | Liverpool Land, East Greenland | 800 | 2.5 | 0 | 0 | 0.0375 | 0.816 | 0.996 |
| 0.392 | Granulite, Hongseong, South Korea | 890 | 1.7 | 0 | 0 | 0.0148 | 0.731 | 0.992 |
| 0.391 | Granulite, Yushugou, southeastern Tienshan, China | 980 | 1.4 | 0 | 0 | 0.000457 | 0.534 | 0.981 |
| 0.389 | Maksyutov Complex, southern Urals | 650 | 3.2 | 0 | 0.000716 | 0.0979 | 0.915 | 0.999 |
| 0.387 | Stary Gieraltów, Śnieżnik Mountains, southwest Poland | 875 | 2.7 | 0 | 0 | 0.0169 | 0.704 | 0.993 |
| 0.384 | Eclogite, Munchberg Massif, Germany | 725 | 3 | 0 | 0.000158 | 0.0552 | 0.858 | 0.998 |
| 0.38 | Międzygórze, Śnieżnik Mountains, southwest Poland | 715 | 2.1 | 0 | 0.000166 | 0.1 | 0.916 | 0.998 |
| 0.38 | Mariánské-Lázně complex, Bohemian Massif, Czech Republic | 640 | 2.75 | 0 | 0.00116 | 0.148 | 0.944 | 0.999 |
| 0.38 | Běstvína granulite, Kutná Hora complex, Bohemian Massif, Czech Republic | 700 | 3.7 | 0 | 0.000226 | 0.0423 | 0.82 | 0.997 |
| 0.365 | Ile de Groix, Armorican Massif, France | 450 | 1.9 | 0.00107 | 0.112 | 0.927 | 0.999 | 1 |
| 0.363 | Lws blueschist, Malpica-Tui Complex, NW Spain | 560 | 2.2 | 4.77×10^{-6} | 0.00743 | 0.461 | 0.987 | 1 |
| 0.36 | Northeastern Connecticut, USA | 1000 | 1 | 0 | 0 | 0 | 0.411 | 0.97 |
| 0.36 | Les Essarts complex, Armorican Massif, France | 700 | 1.6 | 0 | 0.00015 | 0.139 | 0.937 | 0.998 |
| 0.36 | Low-T eclogite, La Varenne, Champocéaux complex, Armorican massif, France | 550 | 1.6 | 4.75×10^{-7} | 0.0128 | 0.602 | 0.992 | 1 |
| 0.358 | Winding Stair Gap, Southern Appalachians, USA | 850 | 0.8 | 0 | 0 | 0.00798 | 0.732 | 0.989 |

| | | | | | | | | |
|-------|--|------|------|-----------------------|-----------------------|----------|-------|-------|
| 0.358 | North-east Greenland, Greenland Caledonides | 970 | 3.6 | 0 | 0 | 0.00455 | 0.464 | 0.984 |
| 0.356 | Chandman, south-west Mongolian Altai, Mongolia | 750 | 0.66 | 0 | 0 | 0.0464 | 0.863 | 0.995 |
| 0.346 | Fosdick migmatite-granite complex, Marie Byrd Land, Antarctica | 740 | 0.7 | 0 | 0 | 0.0599 | 0.88 | 0.995 |
| 0.343 | Eclogite, Blumenau, Erzgebirge, Saxony, Germany | 800 | 3.3 | 0 | 9.36×10^{-7} | 0.0246 | 0.741 | 0.995 |
| 0.342 | Eastern Eger complex, Czech Republic | 850 | 1.6 | 0 | 0 | 0.0256 | 0.853 | 0.994 |
| 0.342 | Granulitgebirge, Saxony, Germany | 1010 | 2.2 | 0 | 0 | 0.00135 | 0.481 | 0.981 |
| 0.342 | Kyanite eclogite, T-7 borehole, Ceske stredohori Mtns, Bohemian Massif, Czech Republic | 970 | 3.8 | 0 | 0 | 0.00434 | 0.444 | 0.983 |
| 0.342 | Stráž nad Ohří, Eger complex, Czech Republic | 1100 | 4.8 | 0 | 0 | 0.000521 | 0.191 | 0.954 |
| 0.341 | Drill core from borehole at Tirschheim, Granulitgebirge, Saxony, Germany | 1010 | 2.25 | 0 | 0 | 0.00145 | 0.48 | 0.981 |
| 0.341 | Erzgebirge, Saxony, Germany | 830 | 2.1 | 0 | 0 | 0.0321 | 0.804 | 0.995 |
| 0.34 | Central Vosges, NE France | 925 | 1.3 | 0 | 0 | 0.00442 | 0.653 | 0.987 |
| 0.34 | Argentera Massif, Italy | 735 | 1.38 | 0 | 0 | 0.0983 | 0.914 | 0.997 |
| 0.338 | Le Conquet Schist, Leon Domain, French Massif Armoricaïn | 675 | 0.7 | 0 | 0 | 0.157 | 0.94 | 0.998 |
| 0.335 | Central Schwarzwald granulite complex, Germany | 950 | 1.55 | 0 | 0 | 0.00353 | 0.615 | 0.986 |
| 0.33 | Ulten zone, Eastern Alps | 700 | 1.5 | 0 | 0.000105 | 0.142 | 0.938 | 0.998 |
| 0.325 | Golfe du Morbihan, Brittany, France | 800 | 0.8 | 0 | 0 | 0.0258 | 0.816 | 0.993 |
| 0.32 | UHP eclogite, southwestern Tienshan, China | 505 | 3.2 | 7.61×10^{-5} | 0.0102 | 0.514 | 0.99 | 1 |
| 0.32 | Coe metapelite, southwestern Tienshan, China | 565 | 2.9 | 7.19×10^{-6} | 0.00402 | 0.31 | 0.977 | 1 |
| 0.32 | Lws eclogite, southwestern Tienshan, China | 498 | 2.43 | 0.000158 | 0.0232 | 0.71 | 0.996 | 1 |
| 0.319 | Atbashy, Tienshan, Kyrgyzstan | 600 | 2.4 | 0 | 0.00301 | 0.279 | 0.973 | 1 |
| 0.318 | HP eclogite, southwestern Tienshan, China | 565 | 2.35 | 3.70×10^{-6} | 0.00608 | 0.403 | 0.985 | 1 |
| 0.316 | Ivrea zone, Italy | 910 | 1.1 | 0 | 0 | 0.00393 | 0.663 | 0.987 |
| 0.315 | Eclogite, Montagne Noire, French Massif Central | 725 | 1.4 | 0 | 0 | 0.11 | 0.922 | 0.998 |
| 0.315 | Eclogite, Shanderman, northern Iran | 605 | 1.8 | 0 | 0.00363 | 0.347 | 0.979 | 1 |
| 0.308 | Eastern Montagne Noire, Massif Central, France | 725 | 0.8 | 0 | 0 | 0.0869 | 0.905 | 0.996 |
| 0.3 | Pichilemu, central Chile | 555 | 0.42 | 0 | 0.00351 | 0.553 | 0.985 | 0.999 |
| 0.299 | Altai, Chinese Altai, Central Asian orogenic belt, China | 660 | 0.63 | 0 | 0 | 0.179 | 0.946 | 0.998 |
| 0.28 | Val Malenco, north Italy | 850 | 1.05 | 0 | 0 | 0.0162 | 0.769 | 0.992 |
| 0.278 | Kalasu, Chinese Altai, Central Asian orogenic belt, China | 950 | 0.8 | 0 | 0 | 0 | 0.495 | 0.975 |
| 0.277 | Fuyun, Chinese Altai, Central Asian orogenic belt, China | 970 | 0.9 | 0 | 0 | 0 | 0.471 | 0.974 |
| 0.274 | Sumdo eclogite, Lhasa block, Tibet | 670 | 2.7 | 0 | 0.000657 | 0.112 | 0.926 | 0.999 |
| 0.272 | Gruf complex, central Alps | 920 | 0.9 | 0 | 0 | 0.000519 | 0.604 | 0.983 |
| 0.265 | Eclogite, Jilang, Lhasa block, Tibet | 770 | 3.6 | 0 | 3.03×10^{-5} | 0.0257 | 0.743 | 0.995 |
| 0.261 | Eclogite, Songdo, Lhasa block, Tibet | 730 | 2.7 | 0 | 0.00013 | 0.0634 | 0.875 | 0.998 |
| 0.257 | Qianjin eclogite, Huwan Shear Zone, Hong'An, China | 575 | 2.4 | 6.77×10^{-7} | 0.00484 | 0.363 | 0.982 | 1 |
| 0.253 | Granulite, Imjingang Belt, South Korea | 900 | 2 | 0 | 0 | 0.0138 | 0.709 | 0.991 |
| 0.252 | Xiongdian eclogite, Huwan Shear Zone, Hong'An, China | 610 | 2.3 | 0 | 0.00263 | 0.264 | 0.971 | 0.999 |
| 0.242 | Blueschist, Lancang tectonic belt, Southwest China | 390 | 1 | 0.0158 | 0.632 | 0.994 | 1 | 1 |

| | | | | | | | | |
|-------|---|-----|------|-----------------------|-----------------------|---------|-------|-------|
| 0.242 | Lawsonite blueschist, northwestern Qiangtang, Tibet | 375 | 1.05 | 0.0285 | 0.752 | 0.996 | 1 | 1 |
| 0.236 | Huangzhen-Zhujiachong, South Dabie zone, China | 670 | 3.3 | 0 | 0.000472 | 0.0745 | 0.89 | 0.998 |
| 0.236 | Weihai, Sulu belt, China | 660 | 3 | 0 | 0.000689 | 0.102 | 0.918 | 0.999 |
| 0.236 | Taohang, Sulu belt, China | 700 | 3.4 | 0 | 0.00025 | 0.0524 | 0.85 | 0.998 |
| 0.235 | Gangma Co, central Qiangtang, Tibet | 435 | 2.25 | 0.00134 | 0.127 | 0.936 | 0.999 | 1 |
| 0.233 | Shuanghe (eclogite/marble), medium-T UHP eclogite zone, Dabie Shan, China | 726 | 4.1 | 0 | 0.000119 | 0.0256 | 0.733 | 0.996 |
| 0.233 | Yangkou, Sulu belt, China | 733 | 3.5 | 0 | 0.000111 | 0.0368 | 0.801 | 0.997 |
| 0.233 | Marble, Sanqingge, Sulu belt, China | 600 | 3.55 | 5.99×10^{-7} | 0.00131 | 0.132 | 0.938 | 0.999 |
| 0.231 | Eclogite, Gyeonggi Massif, South Korea | 840 | 2 | 0 | 0 | 0.0293 | 0.796 | 0.995 |
| 0.23 | Bailang eclogite, Lhasa block, Tibet | 490 | 2.6 | 0.000183 | 0.0242 | 0.717 | 0.996 | 1 |
| 0.23 | Song Ma suture zone, northern Vietnam | 700 | 2.6 | 0 | 0.000333 | 0.0889 | 0.907 | 0.998 |
| 0.227 | Xinxian, low-T UHP eclogite unit, western Dabieshan, China | 610 | 2.9 | 0 | 0.0018 | 0.186 | 0.957 | 0.999 |
| 0.227 | Luotian, North Dabie zone, China | 970 | 4.25 | 0 | 0 | 0.00381 | 0.397 | 0.981 |
| 0.227 | Eclogite, Donghai, Sulu belt, China | 660 | 3.3 | 0 | 0.000568 | 0.0823 | 0.9 | 0.999 |
| 0.223 | Rongma, central Qiangtang, Tibet | 520 | 1.4 | 4.05×10^{-5} | 0.0275 | 0.754 | 0.996 | 1 |
| 0.218 | Pinchi Lake, British Columbia, Canada | 536 | 2.55 | 3.51×10^{-5} | 0.00932 | 0.502 | 0.99 | 1 |
| 0.202 | Basong Tso complex, North Lhasa terrane, China | 690 | 0.9 | 0 | 0 | 0.15 | 0.938 | 0.998 |
| 0.191 | Mafic granulite lens in gneiss of Amdo metamorphic complex, Tibet | 890 | 1.51 | 0 | 0 | 0.0133 | 0.73 | 0.991 |
| 0.19 | Eclogite, Basu, Qiangtang, central Tibet | 990 | 4 | 0 | 0 | 0.00327 | 0.394 | 0.98 |
| 0.179 | Amdo metamorphic complex, Tibet | 650 | 0.9 | 0 | 0.000197 | 0.243 | 0.962 | 0.999 |
| 0.158 | Kimi complex, Rhodope zone, Greece | 800 | 4 | 0 | 9.96×10^{-6} | 0.0161 | 0.648 | 0.993 |
| 0.158 | Eclogite, Ring Mountain, Tiburon Peninsular, California, USA | 585 | 2.35 | 0 | 0.00413 | 0.335 | 0.979 | 1 |
| 0.15 | Raft River Mountains, Sevier hinterland, USA | 600 | 0.7 | 0 | 0.0031 | 0.398 | 0.978 | 0.999 |
| 0.145 | Cazadero, Northern California, USA | 504 | 1.8 | 0.000155 | 0.0322 | 0.776 | 0.997 | 1 |
| 0.145 | Jenner, Northern California, USA | 435 | 2.2 | 0.00139 | 0.132 | 0.938 | 0.999 | 1 |
| 0.14 | Northeastern Nicaragua | 590 | 1.6 | 0 | 0.00531 | 0.427 | 0.984 | 1 |
| 0.132 | Albion Mountains, Sevier hinterland, USA | 600 | 0.65 | 0 | 0.00122 | 0.388 | 0.977 | 0.999 |
| 0.132 | Carrizal Grande, south Motagua Fault Zone, Guatemala | 520 | 2.5 | 6.96×10^{-5} | 0.0135 | 0.59 | 0.993 | 1 |
| 0.127 | Breaksea orthogneiss, Fjordland, New Zealand | 850 | 1.8 | 0 | 0 | 0.0263 | 0.789 | 0.994 |
| 0.124 | Lws eclogite, Bantimala complex, south Sulawesi, Indonesia | 580 | 2.6 | 6.23×10^{-7} | 0.00383 | 0.311 | 0.977 | 1 |
| 0.118 | Luk Ulo complex, central Java, Indonesia | 440 | 2.2 | 0.00119 | 0.116 | 0.929 | 0.999 | 1 |
| 0.115 | Fosdick migmatite-granite complex, Marie Byrd Land, Antarctica | 870 | 0.75 | 0 | 0 | 0.00278 | 0.679 | 0.986 |
| 0.113 | Doubtful Sound, Fjordland, New Zealand | 920 | 1.4 | 0 | 0 | 0.00623 | 0.67 | 0.988 |
| 0.104 | Jagua Clara melange, Rio San Juan complex, Dominican Republic | 585 | 2.3 | 0 | 0.00427 | 0.344 | 0.98 | 1 |
| 0.1 | Yanai, Ryole Belt, Japan | 825 | 0.55 | 0 | 0 | 0.00322 | 0.706 | 0.987 |
| 0.096 | Jijal Complex, Pakistan | 875 | 1.2 | 0 | 0 | 0.0125 | 0.741 | 0.991 |
| 0.092 | Pohorje Mountains, Eastern Alps, Slovenia | 820 | 3.7 | 0 | 0 | 0.0166 | 0.664 | 0.993 |
| 0.091 | Sivrihisar massif, central Turkey | 460 | 2.4 | 0.000538 | 0.0593 | 0.864 | 0.998 | 1 |

| | | | | | | | | |
|-------|---|-----|------|-----------------------|-----------------------|--------|-------|-------|
| 0.09 | Koralpe (Hohl), Eastern Alps | 630 | 1.95 | 0 | 0.00202 | 0.253 | 0.968 | 0.999 |
| 0.089 | Eclogite unit, Sanbagawa belt, Japan | 560 | 2 | 2.00×10^{-8} | 0.00843 | 0.496 | 0.989 | 1 |
| 0.086 | Eclogite, Sistan Suture Zone, Iran | 600 | 2.3 | 0 | 0.0032 | 0.294 | 0.975 | 1 |
| 0.085 | Alanya massif, southeastern Turkey | 530 | 1.7 | 3.31×10^{-5} | 0.019 | 0.679 | 0.994 | 1 |
| 0.085 | Druer unit, Sesia Zone, Western Alps | 550 | 1.95 | 8.26×10^{-6} | 0.0107 | 0.55 | 0.991 | 1 |
| 0.084 | Kırşehir-Hirkadağ massifs, Central Anatolia, Turkey | 700 | 0.75 | 0 | 0 | 0.117 | 0.924 | 0.997 |
| 0.083 | Bitlis massif, southeastern Turkey | 520 | 2 | 7.55×10^{-5} | 0.0197 | 0.68 | 0.995 | 1 |
| 0.083 | Tavsanlı zone, western Turkey | 500 | 2.4 | 1.50×10^{-4} | 0.0227 | 0.706 | 0.995 | 1 |
| 0.081 | Garnet Ridge, Colorado Plateau, USA | 630 | 4.07 | 0 | 0.000551 | 0.0625 | 0.87 | 0.998 |
| 0.079 | As Sifah, Oman | 490 | 2.5 | 1.96×10^{-4} | 0.0263 | 0.734 | 0.996 | 1 |
| 0.077 | Chuacús complex, central Guatemala | 705 | 2.25 | 0 | 0.000275 | 0.103 | 0.918 | 0.998 |
| 0.075 | Fondo unit, Sesia Zone, Western Alps | 530 | 1.8 | 3.80×10^{-5} | 0.0179 | 0.665 | 0.994 | 1 |
| 0.071 | Lws blueschist, Seghin, Hajjiabad area, Zagros, | 500 | 1.75 | 1.84×10^{-4} | 0.0365 | 0.797 | 0.997 | 1 |
| 0.069 | Eastern dome, Escambray massif, central Cuba | 600 | 1.6 | 0 | 0.00424 | 0.389 | 0.982 | 1 |
| 0.064 | Priest River core complex, northern Idaho, USA | 785 | 0.95 | 0 | 0 | 0.0428 | 0.852 | 0.995 |
| 0.061 | Western dome, Escambray massif, central Cuba | 470 | 1.5 | 6.34×10^{-4} | 0.0878 | 0.906 | 0.999 | 1 |
| 0.053 | Mabja dome, southern Tibet | 650 | 0.88 | 0 | 0.000162 | 0.241 | 0.961 | 0.999 |
| 0.052 | Syros, Greece | 545 | 2 | 1.54×10^{-5} | 0.0115 | 0.564 | 0.991 | 1 |
| 0.051 | Tso-Morari eclogite, western Himalaya, India | 645 | 2.75 | 0 | 0.00105 | 0.256 | 0.941 | 0.999 |
| 0.051 | Stak eclogite, Haramosh, NE Himalaya, Pakistan | 750 | 2.5 | 0 | 3.95×10^{-5} | 0.0591 | 0.868 | 0.997 |
| 0.05 | Kangmar dome, southern Tibet | 624 | 0.86 | 0 | 0.000941 | 0.323 | 0.972 | 0.999 |
| 0.049 | Voltri Massif, Ligurian Alps | 480 | 2.5 | 0.000269 | 0.0334 | 0.778 | 0.997 | 1 |
| 0.047 | Yardoï dome, southeastern Tibet | 650 | 0.75 | 0 | 5.46×10^{-6} | 0.226 | 0.958 | 0.998 |
| 0.047 | Eclogite, Kaghan Valley, NW Himalaya, Pakistan | 710 | 3.3 | 0 | 0.000216 | 0.0515 | 0.849 | 0.998 |
| 0.045 | Southern Menderes massif, southwestern Turkey | 480 | 1.3 | 0.000416 | 0.0756 | 0.892 | 0.998 | 1 |
| 0.045 | Sifnos, Greece | 550 | 2.2 | 1.33×10^{-5} | 0.00909 | 0.505 | 0.989 | 1 |
| 0.045 | Monviso, Western Alps | 550 | 2.7 | 1.73×10^{-5} | 0.00626 | 0.407 | 0.985 | 1 |
| 0.044 | Zone 4, Pam Peninsula, New Caledonia | 550 | 2.5 | 1.66×10^{-5} | 0.00732 | 0.447 | 0.987 | 1 |
| 0.044 | Lago Di Cignana, Zermatt-Saas zone, Western Alps | 575 | 3 | 2.89×10^{-5} | 0.00307 | 0.26 | 0.98 | 1 |
| 0.044 | Balma unit, Pennine Alps | 580 | 1.9 | 0 | 0.0059 | 0.427 | 0.985 | 1 |
| 0.043 | Gressoney valley, Monte Rosa nappe, Western Alps | 560 | 2.55 | 8.45×10^{-6} | 0.0058 | 0.395 | 0.984 | 1 |
| 0.037 | Shakhdara dome, southern Pamir Mountains | 830 | 1 | 0 | 0 | 0.0218 | 0.796 | 0.99 |
| 0.037 | Trescolmen, Adula nappe, Western Alps | 750 | 2.5 | 0 | 3.95×10^{-5} | 0.0591 | 0.868 | 0.997 |
| 0.036 | Jomolhari massif, western Bhutan | 785 | 0.9 | 0 | 0 | 0.0401 | 0.848 | 0.994 |
| 0.035 | Brossasco-Isasca unit (Dora-Maira Massif), Western Alps | 730 | 4 | 0 | 0.000114 | 0.0267 | 0.742 | 0.996 |
| 0.034 | Day Nui Con Voi metamorphic core complex, northern Vietnam | 805 | 0.85 | 0 | 0 | 0.0262 | 0.815 | 0.993 |
| 0.034 | Gran Paradiso Massif, Western Alps | 520 | 2 | 7.55×10^{-5} | 0.0197 | 0.68 | 0.995 | 1 |
| 0.034 | Schistes Lustrés, Corsica, France | 520 | 2.3 | 7.41×10^{-5} | 0.0158 | 0.629 | 0.994 | 1 |
| 0.034 | Gimigliano, lower ophiolitic unit, Catena Costiera, Calabria, Italy | 370 | 1.25 | 0.0308 | 0.765 | 0.997 | 1 | 1 |
| 0.032 | Ky paragneiss, Kali Gandaki valley, central Nepal | 720 | 1.1 | 0 | 0 | 0.112 | 0.922 | 0.997 |

| | | | | | | | | |
|-------|---|------|-------|-----------------------|-----------------------|----------|-------|-------|
| 0.032 | Eclogite zone, Tauern Window, Eastern Alps, Austria | 560 | 2.55 | 8.45×10^{-6} | 0.0058 | 0.395 | 0.984 | 1 |
| 0.03 | Lower crustal xenoliths, central Mexico | 1020 | 1.15 | 0 | 0 | 0 | 0.386 | 0.969 |
| 0.03 | Higher Himalayan crystalline sequence, Yadong, Tibet | 835 | 1.2 | 0 | 0 | 0.0256 | 0.803 | 0.993 |
| 0.028 | Hunza Valley, Karakoram metamorphic complex, Pakistan | 692 | 0.83 | 0 | 0 | 0.14 | 0.934 | 0.998 |
| 0.028 | Sill-Kfs metatexite, Upper GHC, Nylam, central Himalaya, China | 720 | 0.7 | 0 | 0 | 0.082 | 0.901 | 0.996 |
| 0.027 | Higher Himalayan Crystallines, Sikkim, India | 800 | 1 | 0 | 0 | 0.036 | 0.837 | 0.994 |
| 0.025 | Granulite xenoliths, Kilbourne Hole/Potrillo volcanic field, New Mexico, USA | 875 | 0.845 | 0 | 0 | 0.00435 | 0.692 | 0.987 |
| 0.024 | Paixang, Namche Barwa, eastern Himalaya, China | 850 | 1.5 | 0 | 0 | 0.0247 | 0.791 | 0.993 |
| 0.021 | Oaro Chu Valley, western Bhutan | 710 | 0.65 | 0 | 0 | 0.0882 | 0.906 | 0.996 |
| 0.021 | Eclogite, Arun Valley, eastern Nepal | 670 | 1.5 | 0 | 0.00055 | 0.195 | 0.955 | 0.999 |
| 0.021 | Footwall of the Kef Lakhel thrust, Edough Massif, Algeria | 750 | 3.6 | 0 | 6.75×10^{-5} | 0.03 | 0.768 | 0.996 |
| 0.02 | Eclogite and granulite xenoliths, Dunkeldik magmatic field, central Pamir Mountains | 1060 | 2.7 | 0 | 0 | 0 | 0.349 | 0.972 |
| 0.019 | Hidaka metamorphic belt, Japan | 900 | 0.75 | 0 | 0 | 0.000248 | 0.348 | 0.983 |
| 0.019 | Ky metatexite, Lower GHC, Nylam, central Himalaya, China | 650 | 0.95 | 0 | 5.46×10^{-6} | 0.246 | 0.963 | 0.999 |
| 0.016 | Seram, eastern Indonesia | 925 | 0.9 | 0 | 0 | 0.000295 | 0.591 | 0.982 |
| 0.014 | Eclogite, Dinggye, central Himalaya, China | 750 | 2.1 | 0 | 8.26×10^{-6} | 0.0712 | 0.888 | 0.997 |
| 0.01 | West of Namche Barwa, eastern Himalayan syntaxis | 820 | 1.5 | 0 | 0 | 0.0369 | 0.83 | 0.995 |
| 0.007 | Fergusson Island, eastern Papua New Guinea | 700 | 2.7 | 0 | 3.28×10^{-4} | 0.0837 | 0.902 | 0.998 |
| 0.005 | Yuli belt, eastern Taiwan | 540 | 1.6 | 8.26×10^{-6} | 0.016 | 0.647 | 0.993 | 1 |

Supplement C: Petrographic description of samples

Samples GT1, OSJ1002 and R5 are described in the main text.

KYJ3-2

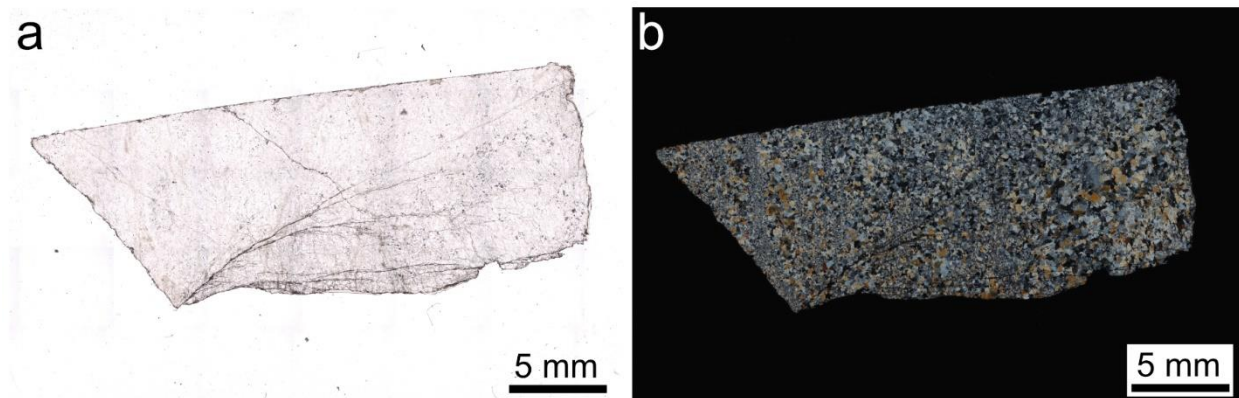


Figure S19 Transmitted-light scans of sample KYJ3-2 in (a) plane- and (b) crossed-polarized light. Acquired using the ZEISS ZEN core software (version 3.6).

Fine-grained jadeitite, entirely made of jadeite grains which includes graphite solid inclusions.

KYJ3-4

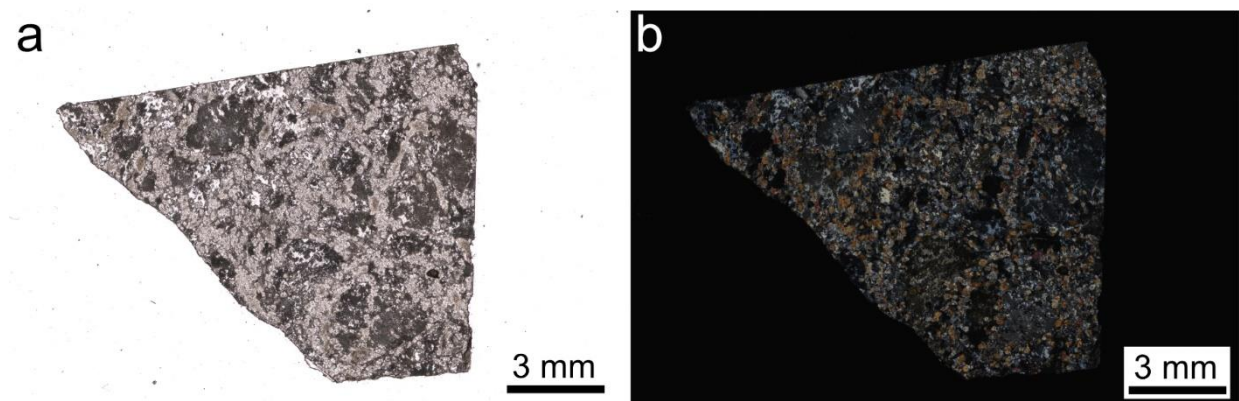


Figure S20 Transmitted-light scans of sample KYJ3-4 in (a) plane- and (b) crossed-polarized light. Acquired using the ZEISS ZEN core software (version 3.6).

Texturally heterogeneous jadeitite, with pseudomorph altered feldspars. Feldspars are replaced by fine-grained zoisite, albite and grossular. Jadeite is fine-grained and seems to replace the primary minerals. The microstructure resembles a substitution texture, rather than a fluid-dominated

texture. In addition to feldspars, albite and jadeite, a single titanite crystal is recognized, which appears to have a core overgrown by a second generation.

FMAB

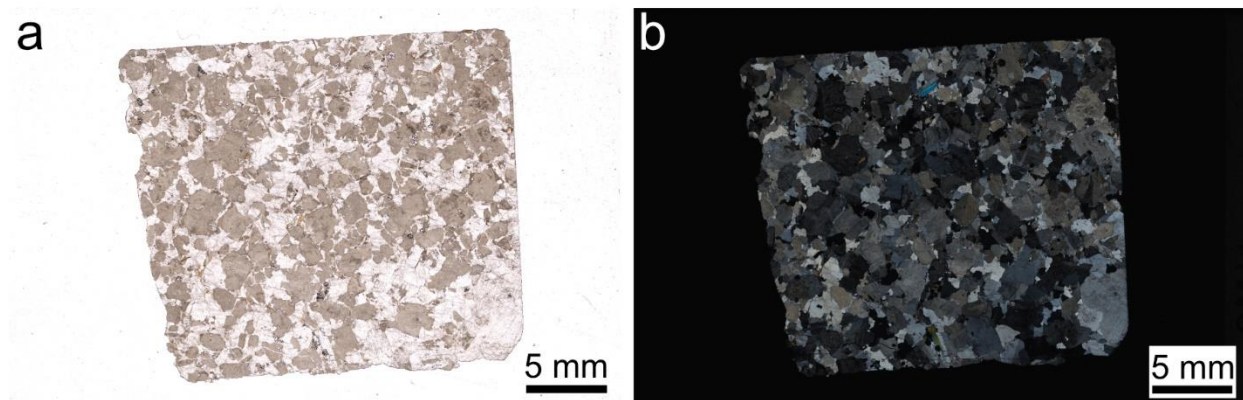


Figure S21 Transmitted-light scans of sample *FMAB* in (a) plane- and (b) crossed-polarized light. Acquired using the *ZEISS ZEN core software* (version 3.6).

Metasomatized coarse-grained granite. Plenty of sericitized plagioclase and K-feldspar grains are recognized, with interstitial quartz and rare muscovite. Primary mafic mineral is biotite, while accessory minerals are zircon and rutile. Secondary minerals are sericite, chlorite and possibly epidote/titanite. There are plenty of euhedral almandine-rich garnet grains, which are often included in feldspar grains, but also found within quartz-dominated domains. Fluid inclusion trails crosscutting quartz grains end against almandine-garnet grain boundaries, indicating that garnet is a later phase than quartz, hence metasomatic. In addition, fluid inclusions in almandine-garnet appear to be mainly primary (i.e., concentric, and parallel to boundaries).

HKJ3

Coarse-grained jadeite-quartz rock, composed of impure jadeite and quartz. Impure jadeite forms radial aggregates of elongate grains. Presence of small-grained opaque minerals, with titanite overgrowth (too tiny for dating), which permits to infer that the opaques are possibly rutile.

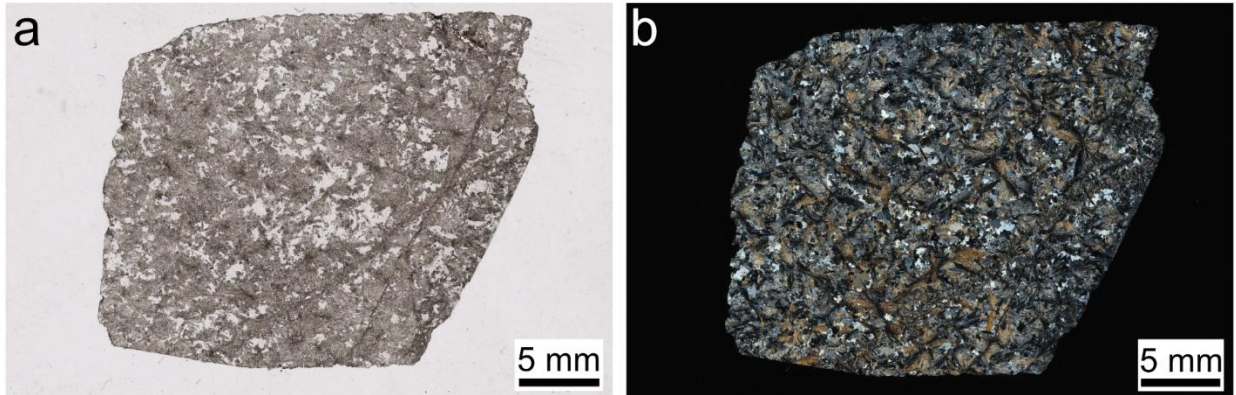


Figure S22 Transmitted-light scans of sample HKJ3 in (a) plane- and (b) crossed-polarized light. Acquired using the ZEISS ZEN core software (version 3.6).

HKJ2

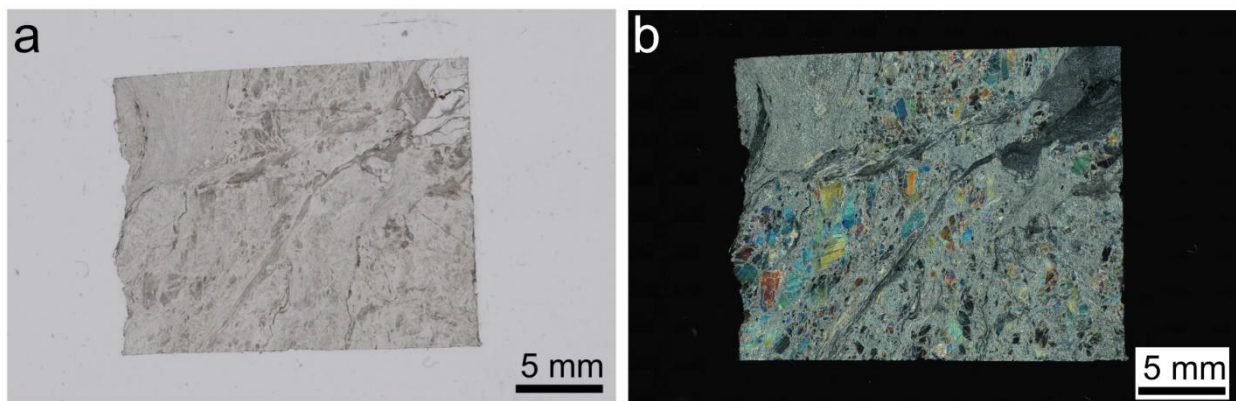


Figure S23 Transmitted-light scans of sample HKJ2 in (a) plane- and (b) crossed-polarized light. Acquired using the ZEISS ZEN core software (version 3.6).

Fine-grained, intensely deformed diopside-rich metasomatic rock (“diopsidite”). In addition to fine-grained diopside, banalsite-stronalsite is present. The rock is locally cut by ultramylonites or very fine-grained cataclasites. Some of these levels are chlorite-rich.

Sk3

Fine-grained jadeitite. Other than jadeite, the only mineral recognized is epidote porphyroclasts. The rock is intensely fractured, with fractures crosscutting both jadeite and epidote consistently.

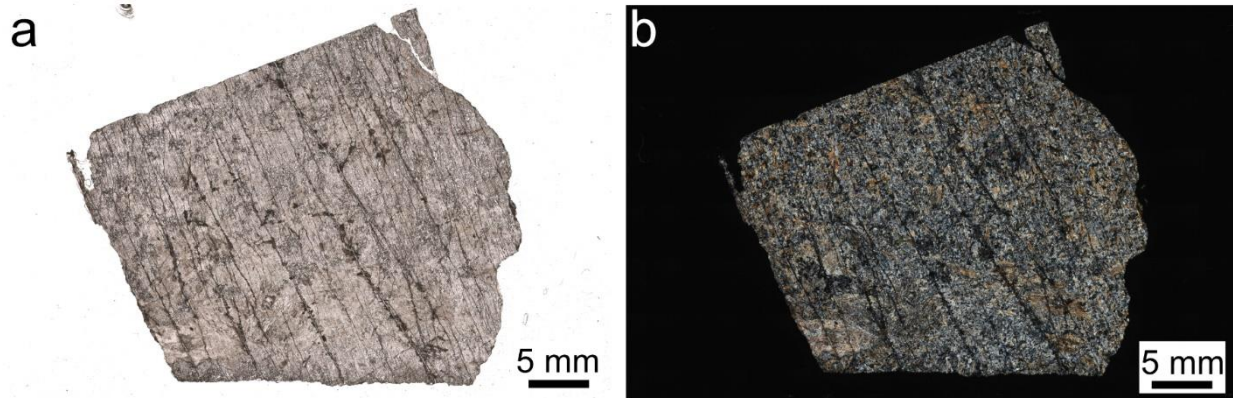


Figure S24 Transmitted-light scans of sample Sk3 in (a) plane- and (b) crossed-polarized light. Acquired using the ZEISS ZEN core software (version 3.6).

FI-3-MYAM

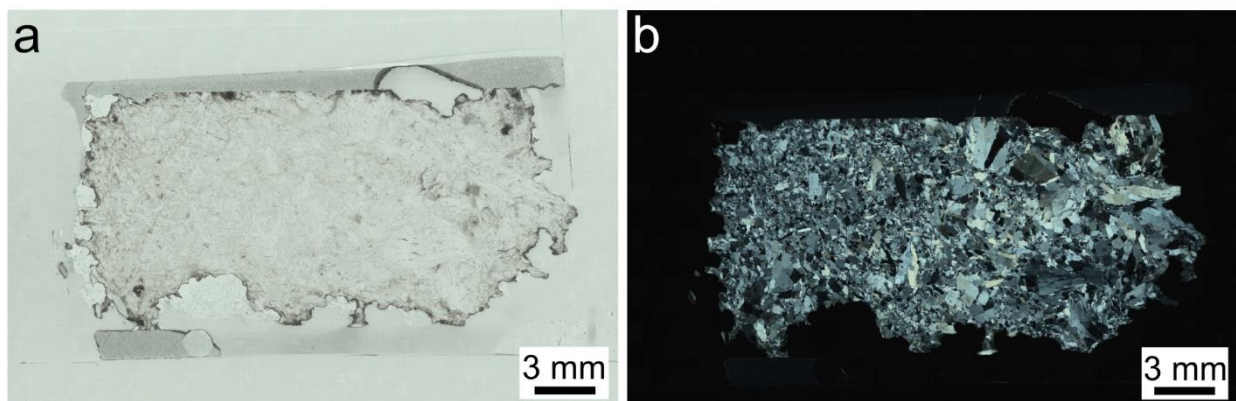


Figure S25 Transmitted-light scans of sample FI-3-MYAM in (a) plane- and (b) crossed-polarized light. Acquired using the ZEISS ZEN core software (version 3.6).

Coarse-grained jadeitite, constituted of jadeite and albite.

KZY-11

Coarse-grained jadeitite entirely made of jadeite. Jadeite grains are mainly elongate. Finer-grained levels are present among coarse-grained jadeite.

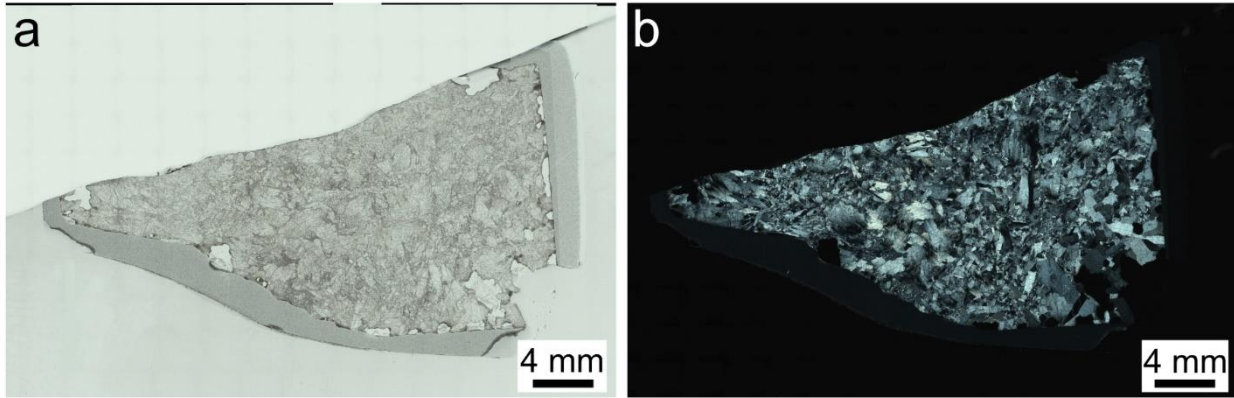


Figure S26 Transmitted-light scans of sample KZY-11 in (a) plane- and (b) crossed-polarized light. Acquired using the ZEISS ZEN core software (version 3.6).

1Bal17-4e1

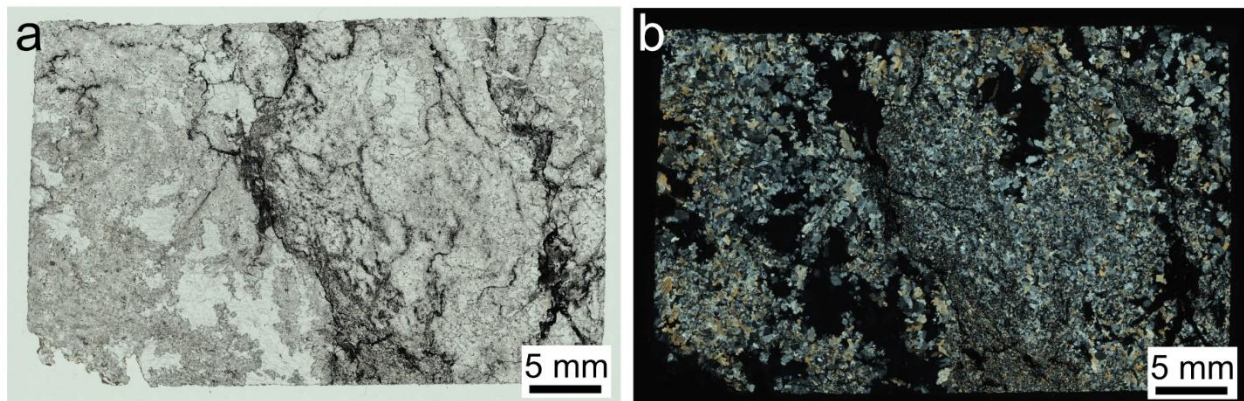


Figure S27 Transmitted-light scans of sample 1Bal17-4e1 in (a) plane- and (b) crossed-polarized light. Acquired using the ZEISS ZEN core software (version 3.6).

Coarse-grained jadeitite made of jadeite and garnet. The rock is intensely crosscut by graphite levels, which are associated with grain-size reduction of jadeite. Although this sample is not presented in any previous work, it is interpreted as a P-type jadeitite because it cements a breccia.

Cfn1

Jadeitite sample entirely made of jadeite, with coarse-grained and mostly elongate grains. The boundary with the country rock is visible, and a thin layer of finer-grained jadeite is present between the main coarse-grained jadeitite and country rock. In this layer, fine-grained, elongate

jadeite grains grow perpendicular to the boundary between the two lithologies. Both jadeitite domains are fractured.

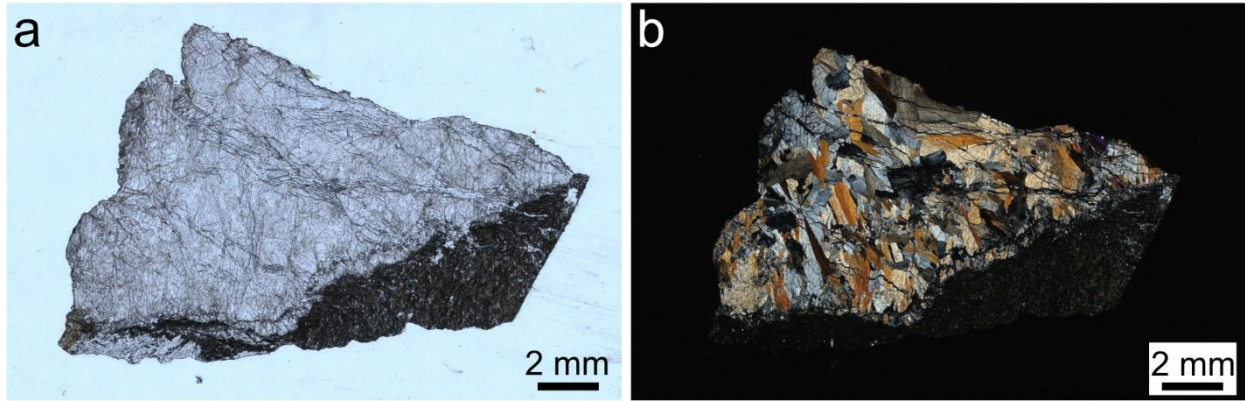


Figure S28 Transmitted-light scans of sample Cfn1 in (a) plane- and (b) crossed-polarized light. Acquired using the ZEISS ZEN core software (version 3.6).

NII

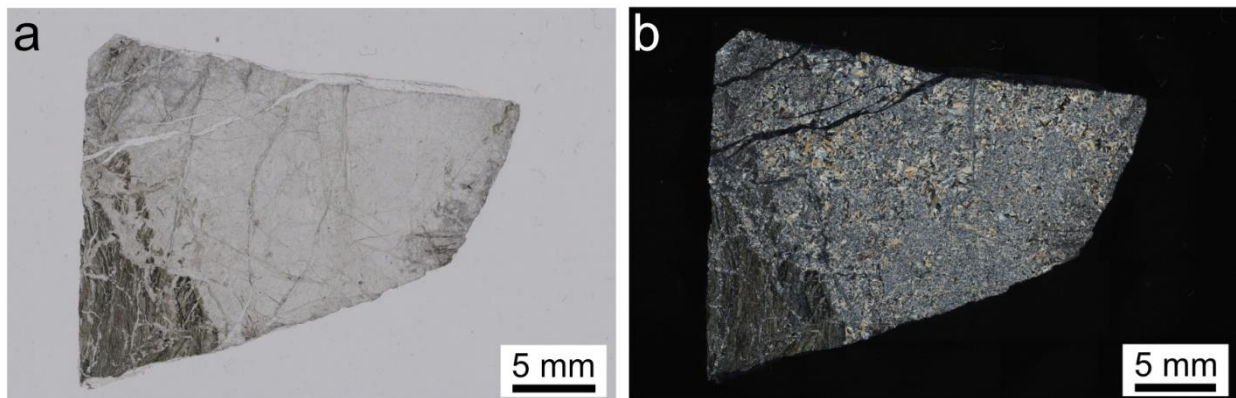


Figure S29 Transmitted-light scans of sample NII in (a) plane- and (b) crossed-polarized light. Acquired using the ZEISS ZEN core software (version 3.6).

Coarse-grained jadeitite entirely made of jadeite that includes graphite. The rock is crosscut by analcime veinlets, which also include graphite. A portion of the country rock, which is recognized as an amphibolite associated with graphite, is visible in thin section.

SYN

Coarse-grained jadeitite entirely composed of jadeite. Rare zircon grains are included in jadeite.

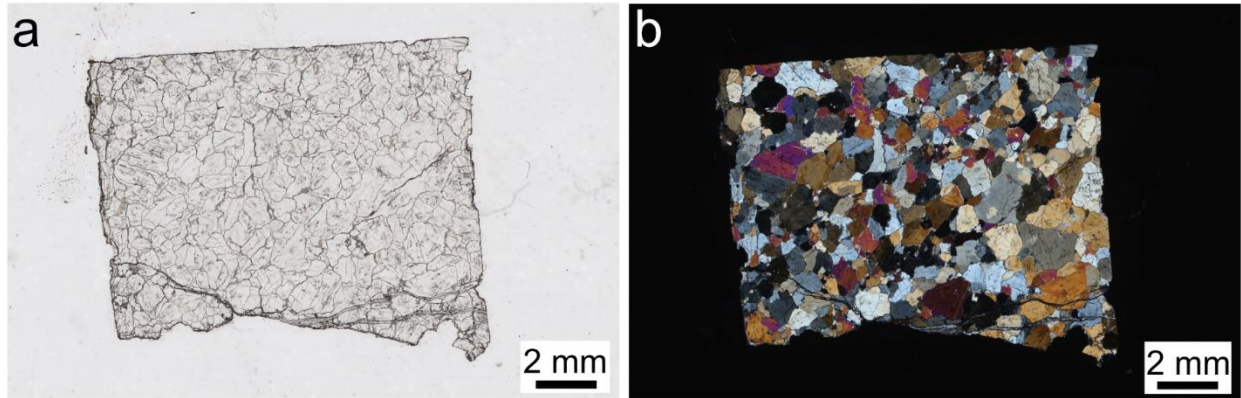


Figure S30 Transmitted-light scans of sample SYN in (a) plane- and (b) crossed-polarized light. Acquired using the ZEISS ZEN core software (version 3.6).

PUL

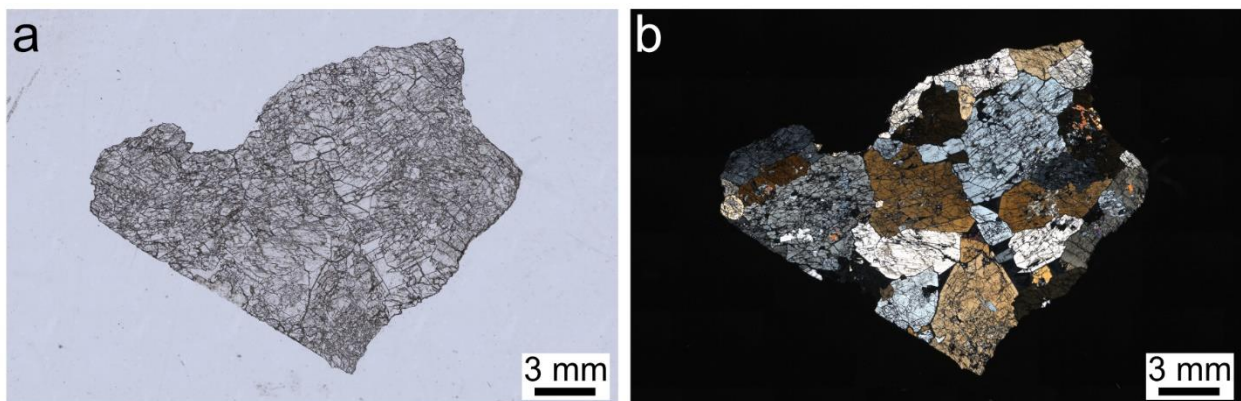


Figure S31 Transmitted-light scans of sample PUL in (a) plane- and (b) crossed-polarized light. Acquired using the ZEISS ZEN core software (version 3.6).

Coarse-grained jadeitite. In addition to jadeite, interstitial garnet, quartz/albite and a few titanite grains are present. Jadeite includes relicts of clinopyroxene. The rock is locally weakly fractured. A fine-grained zircon grain is present, included in jadeite.

RSA1

Medium-grained jadeite. In addition to jadeite, omphacite and albite are present. Finer-grained levels are present, which might be small cataclastic portions.

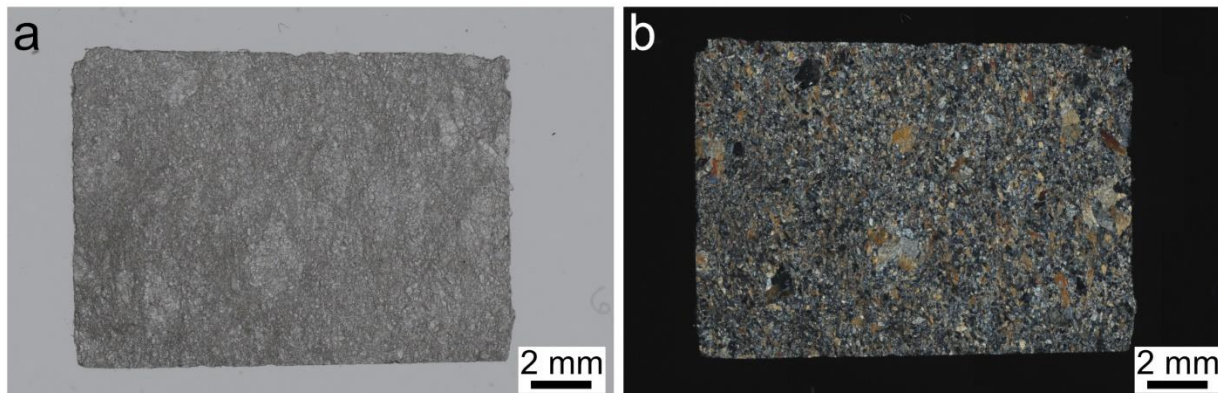


Figure S32 Transmitted-light scans of sample RSA1 in (a) plane- and (b) crossed-polarized light. Acquired using the ZEISS ZEN core software (version 3.6).

References

- Boutier A., Martinez I., Daniel I., Tumiati S., Siron G., Vitale A. and Min I. D. (2024) Computers and Geosciences Thermotopes-COH — A software for carbon isotope modeling and speciation of COH fluids. *Computers and Geosciences* **184**, 105533.
- Brown M. and Johnson T. (2019) Metamorphism and the evolution of subduction on Earth. *American Mineralogist* **104**, 1065–1082.
- Chew D. M., Petrus J. A. and Kamber B. S. (2014) U-Pb LA-ICPMS dating using accessory mineral standards with variable common Pb. *Chemical Geology* **363**, 185–199.
- Elburg M. A., Bons P. D., Foden J. and Brugger J. (2003) A newly defined Late Ordovician magmatic-thermal event in the Mt Painter Province, northern Flinders Ranges, South Australia. *Australian Journal of Earth Sciences* **50**, 611–631.
- Griffin W., Powell W., Pearson N. J. and O'Reilly S. (2008) GLITTER: data reduction software for laser ablation ICP-MS. *Short Course Series* **40**, 308–311.
- Ma Q., Evans N. J., Ling X.-X., Yang J.-H., Wu F.-Y., Zhao Z.-D. and Yang Y.-H. (2019) Natural Titanite Reference Materials for In Situ U-Pb and Sm-Nd Isotopic Measurements by LA-(MC)-ICP-MS. *Geostandards and Geoanalytical Research* **43**, 355–384.
- Spandler C., Hammerli J., Sha P., Hilbert-Wolf H., Hu Y., Roberts E. and Schmitz M. (2016) MKED1: A new titanite standard for in situ analysis of Sm–Nd isotopes and U–Pb geochronology. *Chemical Geology* **425**, 110–126.
- Vermeesch P. (2018) IsoplotR: A free and open toolbox for geochronology. *Geoscience Frontiers* **9**, 1479–1493.